

Distinct patterns of genetic variation at low-recombinant genomic regions represent haplotype structure

Jun Ishigohoka^{1,*} Karen Bascón-Cardozo¹ Andrea Bours¹ Janina Fuß²
Arang Rhie³ Jacquelyn Mountcastle⁴ Bettina Haase⁴ William Chow⁵
Joanna Collins⁵ Kerstin Howe⁵ Marcela Uliano-Silva⁵ Olivier Fedrigo⁴
Erich D. Jarvis^{4,6,7} Javier Pérez-Tris⁸ Juan Carlos Illera⁹
Miriam Liedvogel^{1,10,*}

¹Max Planck Institute for Evolutionary Biology, Plön, Germany

²Institute of Clinical Molecular Biology (IKMB), Kiel University, Kiel, Germany

³Genome Informatics Section, Computational and Statistical Genomics Branch, National Human Genome Research Institute, National Institutes of Health, Bethesda, MD, USA

⁴The Vertebrate Genome Lab, Rockefeller University, New York, NY, USA

⁵Wellcome Sanger Institute, Cambridge, UK

⁶Laboratory of Neurogenetics of Language, Rockefeller University, New York, NY, USA

⁷The Howards Hughes Medical Institute, Chevy Chase, MD, USA

⁸Department of Biodiversity, Ecology and Evolution, Complutense University of Madrid, Madrid, Spain

⁹Biodiversity Research Institute (CSIC-Oviedo University-Principality of Asturias), Oviedo University, Mieres, Spain

¹⁰Institute of Avian Research, Wilhelmshaven, Germany

* Correspondence: Jun Ishigohoka <ishigohoka@evolbio.mpg.de>, Miriam Liedvogel <liedvogel@evolbio.mpg.de>

¹ Abstract

² Genetic variation of the entire genome represents population structure, yet individual loci
³ can show distinct patterns. Such deviations identified through genome scans have often been
⁴ attributed to effects of selective factors instead of randomness, assuming that the genomic
⁵ intervals are long enough to average out randomness in underlying genealogies. However, an
⁶ alternative explanation to distinct patterns has not been fully addressed: too few genealogies
⁷ to average out the effect of randomness. Specifically, distinct patterns of genetic variation
⁸ may be due to reduced local recombination rate, since the number of genealogies in a genomic
⁹ interval corresponds to the number of ancestral recombination events. Here, we associate
¹⁰ distinct patterns of local genetic variation with reduced recombination rate in a songbird, the
¹¹ Eurasian blackcap, using genome sequences and recombination maps. We find that distinct
¹² patterns of local genetic variation represent haplotype structure at low-recombining regions
¹³ present either in all populations or only in a few populations. At the former species-wide low-
¹⁴ recombining regions, genetic variation depicts conspicuous haplotypes segregating in multiple
¹⁵ populations. On the contrary, at the latter population-specific low-recombining regions,
¹⁶ genetic variation primarily represents cryptic haplotype structure among individuals of the
¹⁷ low-recombining populations. With simulations, we confirm that reduction in recombination
¹⁸ rate alone can cause distinct patterns of genetic variation mirroring our empirical data. Our
¹⁹ results highlight that distinct patterns of genetic variation can emerge through evolution of
²⁰ reduced local recombination rate. Recombination landscape as an evolvable trait therefore
²¹ plays an important role determining the heterogeneous distribution of genetic variation along
²² the genome.

23 Introduction

24 Patterns of genetic variation in the genome represent ancestries of sequences and are influenced
25 by population history. While genome-wide genetic variation represents population structure
26 (McVean, 2009; Patterson et al., 2006), randomness in genealogies also contributes to fluctuation
27 of local genetic variation along recombining chromosomes. Specifically, genealogies can differ
28 between loci even under the same population history (Dutheil et al., 2009; Martin & Van
29 Belleghem, 2017; McVean & Cardin, 2005; Pamilo & Nei, 1988; Wakeley, 2008, 2020; Wiuf
30 & Hein, 1999). This is because realisation of a genealogy under a given population history
31 is a probabilistic process: an ancestral haplotype for a set of individuals at one locus is not
32 necessarily a common ancestor of the same set of individuals at another locus (Shipilina et
33 al., 2023). Patterns of local genetic variation along the genome tend to conform with the
34 population structure with random fluctuation (Fig. 1).

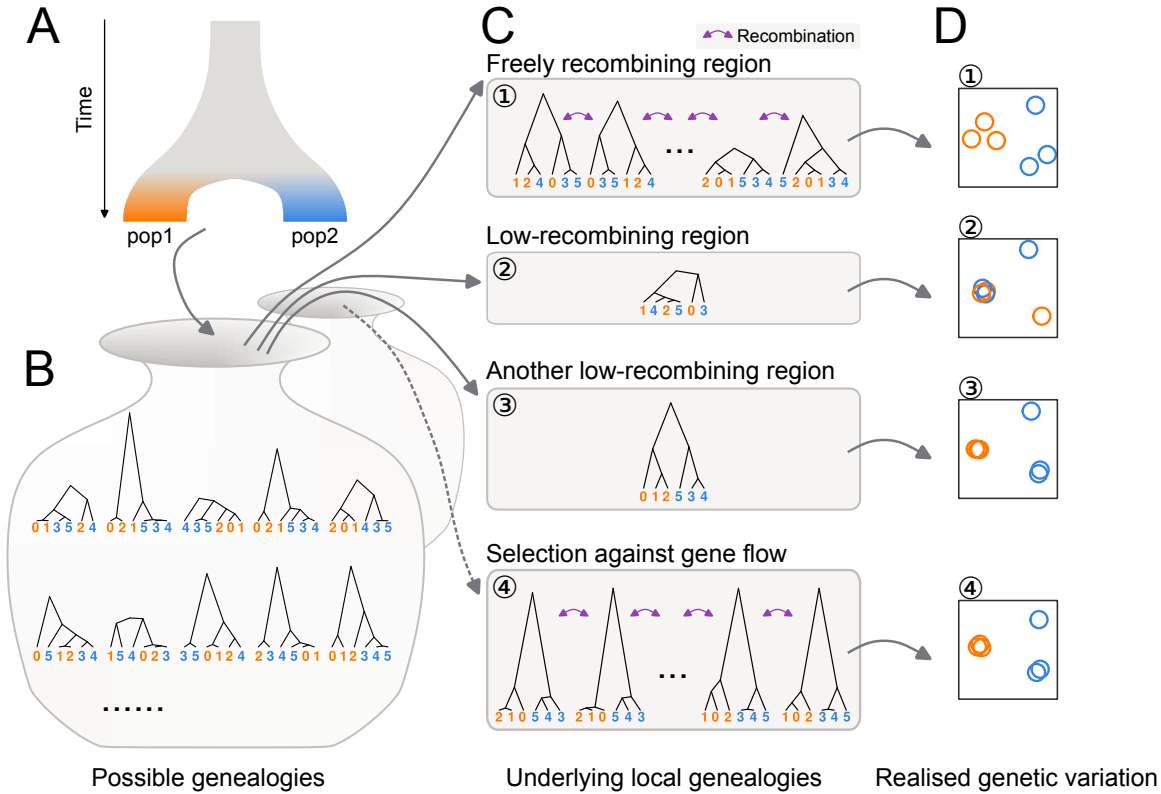


Figure 1: Distinct patterns of genetic variation can be due to reduced recombination rate. Population history (A) affects the distribution of possible genealogies (B) from which local genealogies are drawn (C). The number of genealogies in a genomic interval with a fixed physical length depends on the local recombination rate (C). Mutations occurring on the genealogies (not shown) determine the patterns of realised genetic variation (D). (1) In freely recombining neutral regions, mutations represent many genealogies and hence the pattern of genetic variation converges to the population structure. (2, 3) In low-recombining neutral regions, mutations represent few genealogies covering the region leading to patterns of genetic variation distinct from the population structure. (3) Due to randomness in sampling of genealogies, some of such distinct patterns can be similar to patterns expected at targets of selective factors (c.f. 4). (4) At targets of selection, distribution of possible genealogies is different from that at neutral regions, which is depicted as a different set of possible genealogies in B and the dotted arrow.

35 Inference of population structure as well as other genome-wide analyses based on genetic
 36 variation take advantage of a sufficient number of variable sites (e.g. single nucleotide poly-
 37 morphisms (SNPs)) to eliminate the effect of randomness. One of the most common methods
 38 to summarise population structure based on this approach is principal component analysis
 39 (PCA) applied on a whole-genome genotype table (McVean, 2009; Price et al., 2006). In a
 40 whole-genome PCA, variation among individuals based on variable sites of the entire genome
 41 are projected onto a few major axes, and the distances among individuals on these reduced

42 dimensions represent genetic differences. Summarising population structure and other related
43 measures using the entire genome has been proven to be an effective approach to eliminate
44 random fluctuation of genealogies along the genome (Bhatia et al., 2013; Cao et al., 2020;
45 Fedorova et al., 2013; Peter, 2022; Shao et al., 2023).

46 However, some fundamental biological questions concern selective factors that systemat-
47 ically bias the shape of genealogies at a genomic local scale, shifting the expected patterns
48 of genetic variation from the population structure. For example, patterns of local genetic
49 variation are distinct under selection against gene flow (Fig. 1C4), positive selection and
50 adaptive introgression because they affect coalescence rate, topology, and branch lengths of
51 the underlying genealogies (Hejase et al., 2020; Setter et al., 2020; Speidel et al., 2019; Wolf &
52 Ellegren, 2017). Empirically, genome scans of population genetic summary statistics have been
53 used to identify regions with shifted patterns of genetic variation (Irwin et al., 2018; Martin et
54 al., 2015).

55 Distinct patterns of local genetic variation identified with genome scans are often at-
56 tributed to the effects of selective factors instead of randomness (Burri, 2017; Mérot et al.,
57 2021) based on the assumption that the genomic intervals are large enough to eliminate
58 random fluctuation of genealogies (Li & Ralph, 2019). However, an alternative non-selective
59 explanation is equally conceivable and yet often overlooked: the genomic region may contain
60 an insufficient number of genealogies to eliminate the effect of randomness. Specifically,
61 low-recombining regions may harbour too few genealogies to eliminate the effect of random
62 fluctuation (Lotterhos, 2019).

63 We address the effect of reduced recombination rate on local genetic variation using
64 a songbird species, Eurasian blackcap (*Sylvia atricapilla*, hereafter “blackcap”), which is
65 characterised by variability in seasonal migration across its distribution range (Berthold, 1988,
66 1991; Delmore et al., 2020a; Helbig, 1991). Populations with diverged migratory phenotypes
67 split as recently as ~30,000 years ago, likely corresponding to the last glacial period and
68 now exhibit population structure (Fig. 2A-C, Sup. Fig. 1) (Delmore et al., 2020b). Due
69 to their recent split and relatively large effective population size, genetic differentiation is
70 very low among blackcap populations (Delmore et al., 2020b). The presence of population

71 structure albeit with the low levels of differentiation makes the blackcap a perfect system
72 to investigate local deviations of genetic variation: even the slightest effects of factors that
73 change local genetic variation are likely detectable because such effects are not obscured by
74 population structure. In addition, fine-scale recombination maps for multiple populations
75 are available for this species (Bascón-Cardozo et al., 2022a), facilitating investigation of the
76 relationship between changes in the recombination landscape and locally distinct patterns of
77 genetic variation.

78 By leveraging a large-scale genomic re-sequencing dataset, we first systematically explore
79 distinct patterns of local genetic variation along the blackcap genome, and compare these with
80 genomic regions exhibiting reduced recombination rate. We further investigate the patterns of
81 genetic variation in outlier regions with distinct patterns of genetic variation and associate
82 them with the prevalence of recombination suppression across populations. We also conduct
83 simulations to analyse how reduced local recombination rate in the entire species and in
84 a subpopulation affects patterns of genetic variation through time. Finally, we propose a
85 model of local genetic variation representing haplotype structure corresponding to evolutionary
86 changes in local recombination rate.

87 Results

88 Deviation of genetic variation coincides with low-recombining regions

89 To investigate the genome-wide distribution of genetic variation, we mapped short reads of
90 the whole-genomes of 179 blackcaps including 69 newly sequenced individuals (Sup. Table
91 1) on a *de novo*-assembled reference genome generated through the Vertebrate Genomes
92 Project (VGP, Rhie et al., 2021), and called SNPs ([Materials and Methods](#)). To characterise
93 genome-wide genetic variation, we performed PCA using SNPs in all autosomes, revealing
94 population structure. While PC1 and PC2 represented differentiation of island populations
95 (Fig. 2B), PC3 represented structure within continental populations with different migratory
96 phenotypes (Fig. 2C). To identify genomic regions with patterns of genetic variation distinct
97 from the population structure, we performed local PCA using `lSTRUCT` (Li & Ralph, 2019).

98 Specifically, PCA was performed separately in sliding genomic windows using SNPs, and
99 windows with distinct patterns were identified by evaluating dissimilarity among windows with
100 multidimensionality scaling (MDS). This approach allowed systematic and unbiased exploration
101 unaffected by our definition of populations. By applying a threshold of the MDS values, we
102 identified 32 genomic regions with distinct patterns of genetic variation (hereafter “outlier
103 regions”, Fig. 2D, Sup. Table 3, Sup. Fig. 2). Comparing the genomic distribution of these
104 outlier regions to population-level recombination maps, we found that low-recombinant regions
105 were significantly enriched in the outlier regions (permutation tests, p-value < 0.001 (Sup. Fig.
106 8)). The outlier regions coincided with regions in which recombination rate was reduced either
107 in all tested populations (“species-wide”) or in certain populations (“population-specific”)
108 (Fig. 2E, F, Sup. Fig. 7).

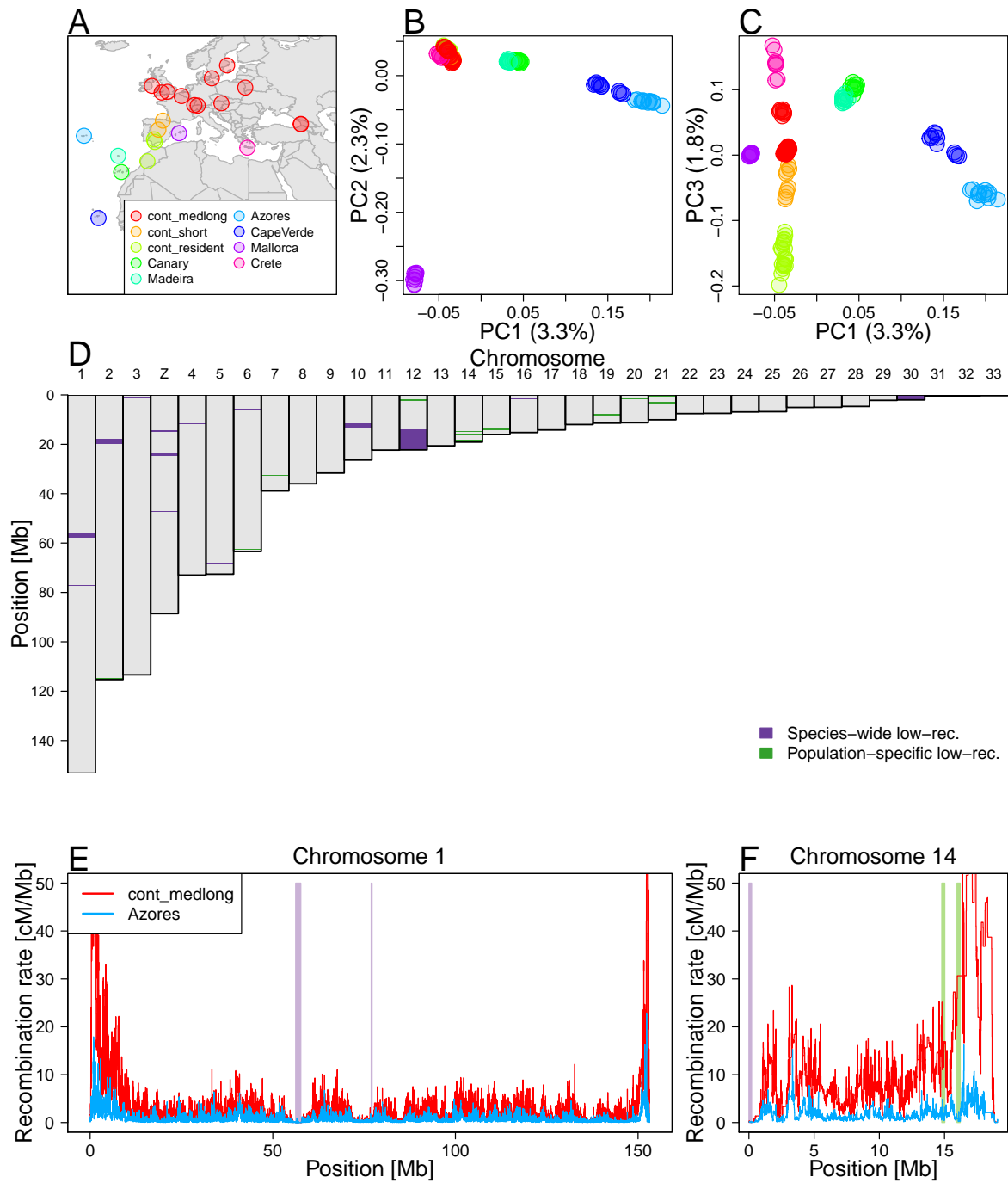


Figure 2: Local PCA outliers coincide with species-wide and population-specific low-recombining regions

A. Geographic location of blackcap populations included in this study. Each point on the map represents a sampling location where multiple individuals were sampled. Populations were defined based on the geographic location, migratory phenotype, and genomic-wide population structure.

B, C. Genome-wide PCA illustrating population structure.

D. Distribution of outlier regions based on local PCA using *lостruct*.

E, F. Inferred recombination rates along two exemplified chromosomes (chromosomes 1 and 14) in two blackcap populations (cont_medlong and Azores). In D-F, purple and green shades respectively indicate positions of outliers that coincide with species-wide and population-specific low-recombining regions.

cont_medlong: medium and long distance migrant population breeding on the continent; cont_short: short distance migrant population breeding on the continent; cont_res: resident (non-migrant) population breeding on the continent. All island populations (Canary, Madeira, Azores, Cape Verde, Mallorca, and Crete) are resident.

109 To further investigate the outlier regions, we separately performed PCA using SNPs in
110 each region, revealing diverse patterns of distinct genetic variation (Fig. 3A-C top). First,
111 species-wide low-recombining regions showed different levels of clustering of individuals in
112 PCA. Specifically, the PCA projections consisted of either three distinct clusters (Fig. 3A
113 top, Sup. Fig. 6), six loose clusters (Fig. 3B top, Sup. Fig. 6), or mixture of all individuals
114 without apparent clustering (Sup. Fig. 6), suggesting that they represent haplotype structure
115 with different numbers of low-recombining alleles. These clusters did not clearly separate
116 populations, indicating a greater contribution of haplotype structure than the population
117 structure. Five of these (e.g. Fig. 3A top, Sup. Figs. 6, 9) had the clearest clustering patterns
118 with three groups of individuals in PCA, which is expected for a haplotype block with two
119 distinct alleles (Huang et al., 2020; Ma & Amos, 2012; Todesco et al., 2020). Two of these
120 regions showed LD patterns consistent with segregating inversions (Fig. 3A bottom, Sup.
121 Fig. 10), and the other three showed patterns of non-inversion haplotype blocks (Sup. Fig.
122 10), indicating that recombination suppression with different mechanisms resulted in similar
123 patterns of genetic variation due to presence of two distinct segregating haplotypes.

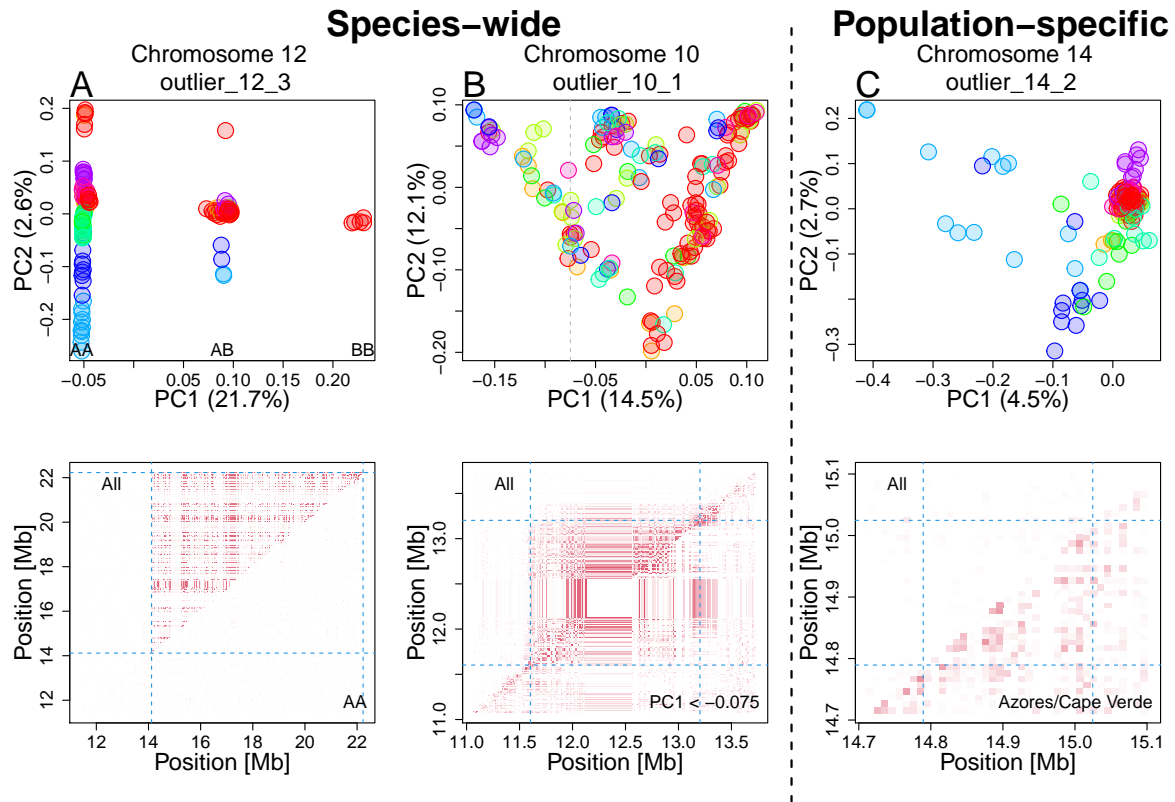


Figure 3: Patterns of genetic variation and linkage disequilibrium at local PCA outliers

Top: PCA at exemplified outlier regions visualising the patterns of local genetic variation. Data points represent blackcap individuals colour-coded by population as depicted in Fig. 2. **Bottom:** LD calculated for all individuals (top-left diagonal) and for subset individuals (bottom-right diagonal).

A. A putative inversion. Three clusters correspond to combination of two non-recombining alleles possessed by individuals, depicted as AA, AB, and BB. LD calculated using AA individuals is not elevated, in line with heterozygote-specific recombination suppression at an inversion locus (Sup. Fig. 12).

B. A species-wide low-recombining region with six loose clusters of individuals. LD calculated using subset individuals was elevated, suggesting genotype-non-specific recombination suppression.

C. A population-specific low-recombining region. The variance in genetic distances between individuals of the low-recombining populations (Azores (blue) and Cape Verde (light blue)) is greater than between other pairs of individuals (top). LD calculated using individuals of the low-recombining populations is elevated (bottom).

124 Second, population-specific low-recombining regions exhibited distinct patterns of genetic
 125 variation consistently across the outlier regions. While individuals from the low-recombining
 126 populations were spread in PCA projections, individuals of other populations were more
 127 densely clustered (Fig. 3C top). This pattern indicates that the variance in genetic distances
 128 between a pair of individuals of the low-recombining populations is greater than between
 129 individuals of normally recombining populations. LD was elevated only in the low-recombining
 130 populations (Fig. 3C bottom), supporting population-specific reduction in recombination rate.

131 **Reduced recombination rate generates distinct patterns of genetic variation**

132 To address whether species-wide and population-specific reduction in recombination rate
133 generates the distinct patterns of genetic variation that we observed above, we performed
134 simulations.

135 First, to investigate the effects of species-wide reduction in local recombination rate, we
136 simulated one ancestral population of 1,000 diploids with a low-recombining genomic region
137 that splits into three subpopulations (pop1, pop2, pop3. Fig. 4A). We sampled individuals
138 over time after the populations split and conducted PCA both in the low-recombining and
139 normally recombining genomic regions. PCA patterns at low-recombining regions (Fig. 4B, C,
140 Sup. Fig. 17) were distinct from normally recombining regions (Fig. 4D). The low-recombining
141 regions exhibited three, six, or more clusters of individuals resembling our empirical results.
142 The clusters of individuals represented genotypes consisting of different combinations of
143 ancestral haplotypes (Sup. Fig. 18). The distinct patterns representing haplotype structure
144 persisted until population structure emerged along the PC axes (Fig. 4B, C). Accordingly, the
145 percentages of variation explained by PC1 and PC2 were higher at low-recombining regions
146 than in normally recombining region until this transition (Fig. 4C). Distinct patterns in the
147 low-recombining regions persisted over longer times than it took for population structure in
148 normally recombining region to emerge (Fig. 4D). These results suggest that distinct patterns
149 of genetic variation in species-wide low-recombining regions represent transient haplotype
150 structure where transition to the population structure is slower than in normally recombining
151 regions.

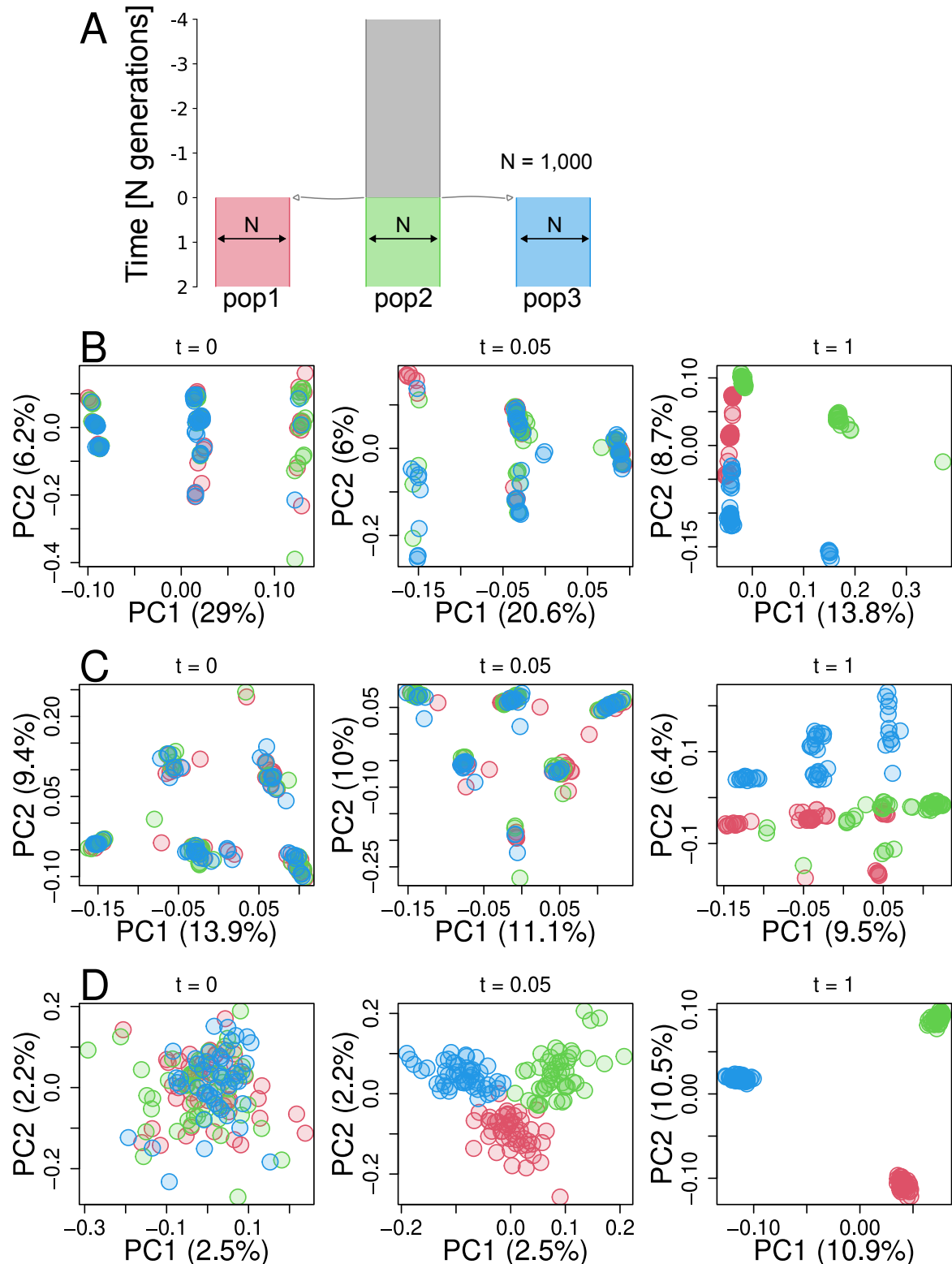


Figure 4: Simulation of a species-wide low-recombing region. **A.** Simulated demography scenario. Our simulated genome contained two chromosomes, one with a low-recombing region and the other without. **B, C.** PCA showing patterns of genetic variation at the species-wide low-recombing region at three time points in three exemplified simulation replicates. **D.** PCA showing patterns of genetic variation at a normally recombining chromosome at three time points in the same replicates as **B**.

152 Second, to investigate the effects of population-specific reduction in local recombination
153 rate, we performed simulations under two scenarios. In both scenarios, three populations
154 (pop1, pop2, and pop3) and their ancestral population had 1,000 diploid individuals, and pop1
155 evolved a reduced local recombination rate. The difference between the two scenarios was the
156 timing of introduction of reduced recombination rate. In the first scenario (Sup. Fig. 19),
157 recombination suppression was introduced at the same time as the three populations split,
158 while in the second scenario (Fig. 5A) recombination suppression was introduced once the
159 three populations differentiated. We conducted PCA in genomic regions with and without
160 population-specific recombination suppression using individuals sampled over time. In both
161 scenarios, the genomic region with population-specific recombination suppression transiently
162 showed distinct patterns of genetic variation (Fig. 5B, Sup. Fig. 19B) resembling the empirical
163 results, while regions without population-specific suppression showed population structure
164 (Fig. 5C). Haplotype structure was not as conspicuous in species-wide low-recombining regions
165 (Sup. Fig. 20B, F, c.f. Sup. Fig. 18) due to standing genetic variation. Mutations originating
166 in the non-recombining population were enriched in the set of mutations that have the greatest
167 contribution to the distinct pattern of PCA (Sup. Fig. 20C, G. χ^2 tests, p-value < 0.001
168 for both models). These mutations were significantly associated with each other in the
169 underlying genealogy sharing common branches compared to other mutations originating in
170 the same population (Sup. Fig. 20D, H. [Materials and Methods](#), Kolmogorov-Smirnov tests,
171 p-value < 0.005 for both models), indicating that the distinct pattern of genetic variation
172 represents sets of mutations that occurred in ancestral haplotypes. Associations between
173 these population-specific mutations on ancestral haplotypes would have eventually decayed by
174 recombination events, but in the low-recombining population the association was maintained
175 due to suppressed recombination, resulting in the cryptic haplotype structure.

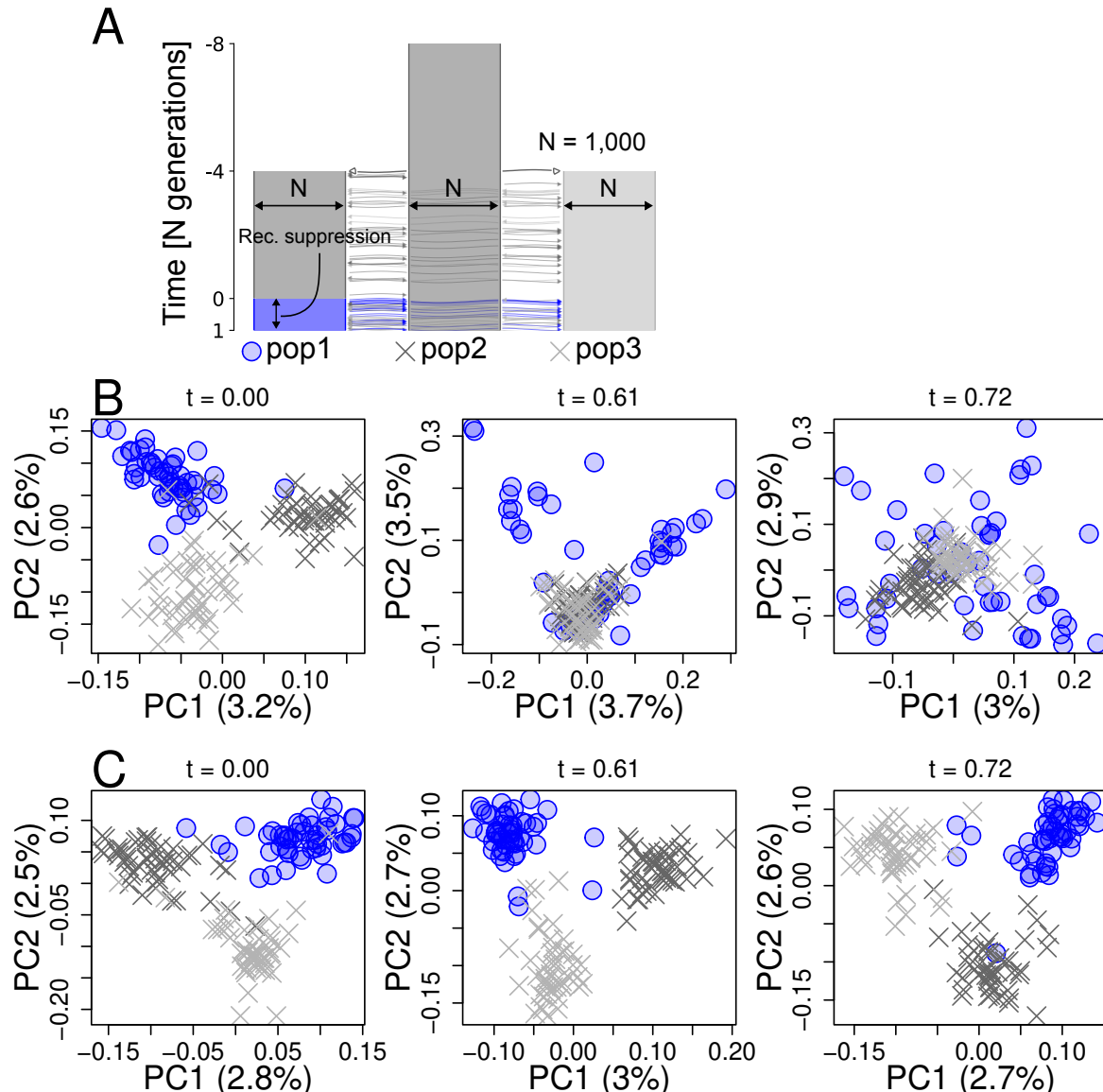


Figure 5: Simulation of a population-specific low-recombing region. **A.** Simulated scenario. Simulated genome contained two chromosomes, one with a population-specific low-recombing region and the other without. **B, C.** PCA showing patterns of genetic variation at the population-specific low-recombing region (**B**) and the normally recombining chromosome (**C**) at three time points in one exemplified simulation replicate.

176 **Effect of selection on patterns of genetic variation**

177 Selection is known to cause distinct patterns of genetic variation (Nielsen, 2005). To test
 178 whether the outlier regions based on `lостruct` identified in the blackcap genome are also
 179 targets of selection, we measured nucleotide diversity (π) and Tajima's D in each population,
 180 as well as ratio between non-synonymous and synonymous substitutions (d_N/d_S) for annotated

181 genes. Many species-wide low-recombining regions showed reduced nucleotide diversity (Sup.
182 Fig. 22) and Tajima's D (Sup. Fig. 21), suggesting that they are under either positive or
183 purifying selection. Most genes within outlier regions had d_N/d_S below 0 (Sup. Fig. 23) with
184 a few genes with positive d_N/d_S , indicating that most genes are under purifying selection and
185 a few others are under positive selection. Furthermore, sequence analysis indicated that some
186 but not all species-wide low-recombining outlier regions coincide with putative pericentromeric
187 regions with enrichment of long tandem repeats (Sup. Figs. 26, 27). These results indicate
188 that the outlier regions may experience effects of selection in addition to reduced recombination
189 rates.

190 We asked whether the distinct patterns of local genetic variation at the outlier regions
191 observed in blackcaps represent the effect of selection or reduced recombination rates. To
192 this end, we simulated positive and purifying selection in with and without reduction in
193 recombination rate (Materials and Methods), and investigated local genetic variation over time
194 by PCA. Overall, representation of haplotype structure in local PCA occurred primarily when
195 recombination rate was reduced at the focal region (Sup. Figs. 24, 25). Decreased genetic
196 diversity due to selection was represented as small dispersal of individuals around a cluster,
197 while variation between non-selected haplotypes, if present, was represented in the primary
198 PC axes. Separation of populations in local PCA at the low-recombining region occurred
199 faster under a higher level of background selection (Sup. Fig. 24). These results indicate that
200 the distinct patterns of genetic variation represented in local PCA primarily reflect haplotype
201 structure due to reduced recombination rate, on which the effect of selection can be overlaid.

202 Discussion

203 A number of empirical population genomics studies have identified ecologically and evolution-
204 arily important genomic regions by locating outlier regions with distinct patterns of genetic
205 variation. Genomic windows in such studies should be ideally both large enough to eliminate
206 the effect of random fluctuation in local genetic variation and small enough to capture the loc-
207 alised signatures of selection. Our results illustrate that distinct patterns of genetic variation in
208 outlier regions based on sliding window approaches can represent haplotype structure reflecting

209 reduced local recombination rates instead of selection. The exact patterns vary depending on
210 the number of haplotypes and prevalence of recombination suppression across populations.
211 Distinct clusters of individuals based on local genetic variation at species-wide low-recombinant
212 regions represent combinations of distinct haplotypes between which shuffling of variation is
213 hindered. Population-specific recombination suppression creates unequal variance in genetic
214 distances between individuals of low-recombinant and normally recombining populations.

215 **Distinct patterns of genetic variation at low-recombinant regions: Genealo-
216 gical interpretations**

217 We discuss our findings from the perspective of underlying genealogies. We first define
218 three terms: (1) genealogical noise, (2) genealogical bias, and (3) mutational noise. (1) By
219 “genealogical noise” we refer to the fact that gene genealogies vary along the genome following
220 a null distribution given a population history (Dutheil et al., 2009; Martin & Van Belleghem,
221 2017; McVean & Cardin, 2005; Wakeley, 2008, 2020; Wiuf & Hein, 1999). (2) By “genealogical
222 bias” we refer to the fact that selective processes can systematically shift the distribution of
223 local genealogies away from the null distribution. For example, genealogies under positive
224 selection, selection against gene flow, adaptive introgression, and balancing selection are biased
225 due to bursts of coalescence, faster lineage sorting, and introduction and maintenance of long
226 branches (Barton & Etheridge, 2004; Guerrero et al., 2012; Hejase et al., 2020; Martin et al.,
227 2019; Setter et al., 2020; Speidel et al., 2019; Taylor, 2013). On top of these, (3) randomness
228 in the process of mutation causes additional noise in realised genetic variation (Ralph et al.,
229 2020), which we call “mutational noise”. For example, the first and the second halves of a
230 chromosomal interval with a single genealogy can still have slightly different patterns of genetic
231 variation because they represent independent sets of mutations. Here we show that distinct
232 patterns of local genetic variation at low-recombinant regions can be explained primarily by
233 haplotype structure due to non-selective genealogical noise instead of selective genealogical
234 bias.

235 We showed that some distinct patterns of genetic variation are associated with species-wide
236 low-recombinant regions. This is in line with previous studies reporting negative correlation

237 between recombination rate and genetic differentiation (Burri et al., 2015). To investigate
238 this relationship in more detail, we performed simulations and demonstrated that haplotype
239 structure underlies the distinct patterns and that it persists only transiently until the effect
240 of the population structure emerges. This transiency reflects a shift from local genetic
241 variation primarily representing haplotype structure (Lotterhos, 2019; Ma & Amos, 2012) to
242 that representing population structure, which can be interpreted based on the underlying
243 genealogies. Low-recombining regions have few underlying genealogies and haplotype structure
244 at such regions tend to reflect their basal branches because basal branches tend to be longer
245 than peripheral branches. At a time point soon after a population split event, peripheral
246 branches covering more recent times than the population split harbour fewer mutations than
247 basal branches. Therefore, the realised pattern of genetic variation at this stage has the greatest
248 contributions by mutations on the long basal branches undifferentiated among populations
249 (i.e. consisting standing genetic variation), representing a few ancestral haplotypes that descend
250 the current sample. As time passes after the population split, the proportion of mutations that
251 have occurred after the population split increases while some ancestral haplotypes can be lost
252 by chance (i.e. drift), increasing the contribution of population structure on genetic variation.
253 This type of distinct patterns of genetic variation arises predominantly in low-recombining
254 regions but less so in normally recombining regions. This is because haplotype structure
255 representing a few ancestral lineages would become less prominent with recombination as
256 different segments of a current haplotype can follow distinct ancestries and thus the genealogical
257 noise is effectively averaged out.

258 Some low-recombining regions may have genealogies with much shorter basal branches than
259 other low-recombining regions because the variance in the basal branch length is greater than
260 peripheral branches (Wakeley, 2008). The over-representation of a few ancestral haplotypes
261 in genetic variation requires long basal branches in the underlying genealogies, and thus
262 low-recombining regions with relatively short basal branches cannot accommodate sufficient
263 mutations to represent distinct ancestral haplotypes. This decreases the relative contribution of
264 genealogical noise compared to mutational noise (Supplementary Notes 1.1). Distinct patterns
265 of genetic variation with varying levels of clustering of individuals in PCA in our empirical

266 results may correspond to different ratios between genealogical and mutational noise due to
267 large variance in the basal branch lengths of underlying genealogies. Specifically, some outlier
268 regions with mixture of individuals from multiple populations without distinct clusters and
269 population subdivision in PCA may have underlying genealogies with short basal branches
270 leading to greater contributions of mutational noise on the realised genetic variation.

271 We both empirically and with simulations showed that population-specific low-recombining
272 regions exhibit distinct patterns of genetic variation in which individuals of low-recombining
273 and normally recombining populations have different variance in genetic distances. This
274 unequal variance in low-recombining and normally recombining populations can be interpreted
275 based on the underlying genealogies (Sup. Fig. 28). We consider the ancestry of current
276 samples of low-recombining and normally recombining populations and split the ancestry at
277 the time T when the population-specific recombination suppression initiated (Sup. Fig. 28A).
278 At time T , there were n ancestral haplotypes that descend all current samples. At times older
279 than T , the ancestors of these n haplotypes freely recombine, making the genetic distances
280 among the ancestral haplotypes close to equidistant (Sup. Fig. 28B). After the initiation of the
281 population-specific reduction in recombination rate, the ancestry of one current sequence of
282 the low-recombining population can be traced back to either one of the n ancestral haplotypes
283 present at the time T (Sup. Fig. 28A). On the contrary, the ancestry of one current sequence
284 of the normally recombining population can be traced back to multiple ancestral haplotypes
285 of the n sequences because of the presence of recombination (Sup. Fig. 28A). From the
286 perspective of mutations, in the low-recombining population, mutations that arose on the same
287 haplotype tend to be linked until the present time because of the suppressed recombination.
288 On the other hand, in the normally recombining population, mutations that arose on the same
289 ancestral haplotype less likely stay linked until the present time because recombination can
290 dissociate them. Because shuffling of haplotypes reduces the variance of genetic distances
291 among sequences, population-specific reduction in recombination rates leads to greater variance
292 in low-recombining population than in normally recombining population as observed in our
293 empirical results and simulations. In short, because of the different recombination rates
294 between the populations, genealogical noise is more efficiently eliminated in the normally

295 recombining population than in the low-recombining population.

296 We also demonstrated with simulations that distinct patterns of genetic variation at
297 population-specific low-recombining regions represent cryptic haplotype structure within the
298 low-recombining population. The haplotype structure is only cryptic and less apparent than
299 in species-wide low-recombining regions because other standing mutations coexist on the
300 same haplotype, which are older than the initiation of the population-specific recombination
301 suppression. The elevated PC loadings at linked mutations originating in the low-recombining
302 population could be informative to study evolutionary change in local recombination rate: the
303 ages of such mutations mapped on inferred genealogies might be useful to estimate the timing
304 at which the population-specific recombination suppression initiated.

305 In our empirical analyses in blackcaps, we detected the effect of population-specific
306 reduction of recombination rate in Azores and Cape Verde island populations. It remains
307 unclear why reduced recombination rate in certain populations but not others is reflected as
308 distinct patterns of genetic variation by *lostruct*. The recent split of Azores and Cape Verde
309 populations from other populations, accompanied by reduction in population size and the level
310 of isolation (Delmore et al., 2020b) may have contributed to more efficient spread of reduced
311 recombination rate.

312 **Recombination landscape as a driver of evolution of local genetic variation**

313 Species-wide and population-specific recombination suppression underlying distinct patterns
314 of local genetic variation are probably not independent: reduction in recombination rates that
315 initiates formation of haplotype blocks likely originates from one population and may spread
316 to multiple populations. For example, local recombination rate may be initially reduced in
317 one population in which a segregating inversion originates before it may spread in multiple
318 populations by gene flow (Faria et al., 2019). In line with this view of recombination map
319 as an evolvable trait diverging across populations according to subdivision, recent studies
320 find that divergence in local recombination rate among populations is correlated with genetic
321 divergence (Bascón-Cardozo et al., 2022a; Spence & Song, 2019). Future work on the effects
322 of transition from population-specific to species-wide suppression of recombination will fill the

323 gap between the two states.

324 Besides spread of recombination suppression across populations, there are other paths
325 along which patterns of local genetic variation may change over time. First, change in
326 frequency of one haplotypic variant by drift or gene flow and selection and accumulation
327 of novel mutations may shift the distinct pattern of genetic variation (Rubin et al., 2022).
328 Second, an increase in recombination rate in the region may resolve the distinct pattern of
329 genetic variation and result in emergence of the population structure, because recombination
330 breaks down discrete haplotypes and generates mixed types whereby reducing the variance
331 of genetic variation (Hudson, 1983). These two types of shifts in distinct patterns of genetic
332 variation are not mutually exclusive. For example, fixation of an inversion results in elevated
333 recombination rate (Smukowski Heil et al., 2015; Steviston et al., 2011) because there are
334 no longer non-recombining heterozygotes in the population. Due to resumed recombination,
335 patterns of local genetic variation in such regions are expected to reflect population structure
336 eventually. The question of how long it takes for an outlier region with distinct patterns of
337 genetic variation to disappear after these events should be focially studied in the future.

338 In Fig. 6A, we illustrate a model for the evolution of local genetic variation that changes
339 according primarily to the evolution of local recombination rates. Local genetic variation
340 can become distinct from the population structure first by representing emerging haplotype
341 structure associated with population-specific recombination suppression or other types of
342 haplotype blocks (e.g. inversions) in one population. If this recombination suppression spreads
343 throughout all populations, then local genetic variation will start to reflect species-wide
344 haplotype structure. Once the relative contribution of haplotype structure on local genetic
345 variation is reduced by differentiation or disappears by elevated recombination rates, then
346 genetic variation returns to reflect the population structure and consequently the outlier
347 region disappears. The effect of selection on local genetic variation may be overlaid on top
348 (Supplementary Notes 1.2).

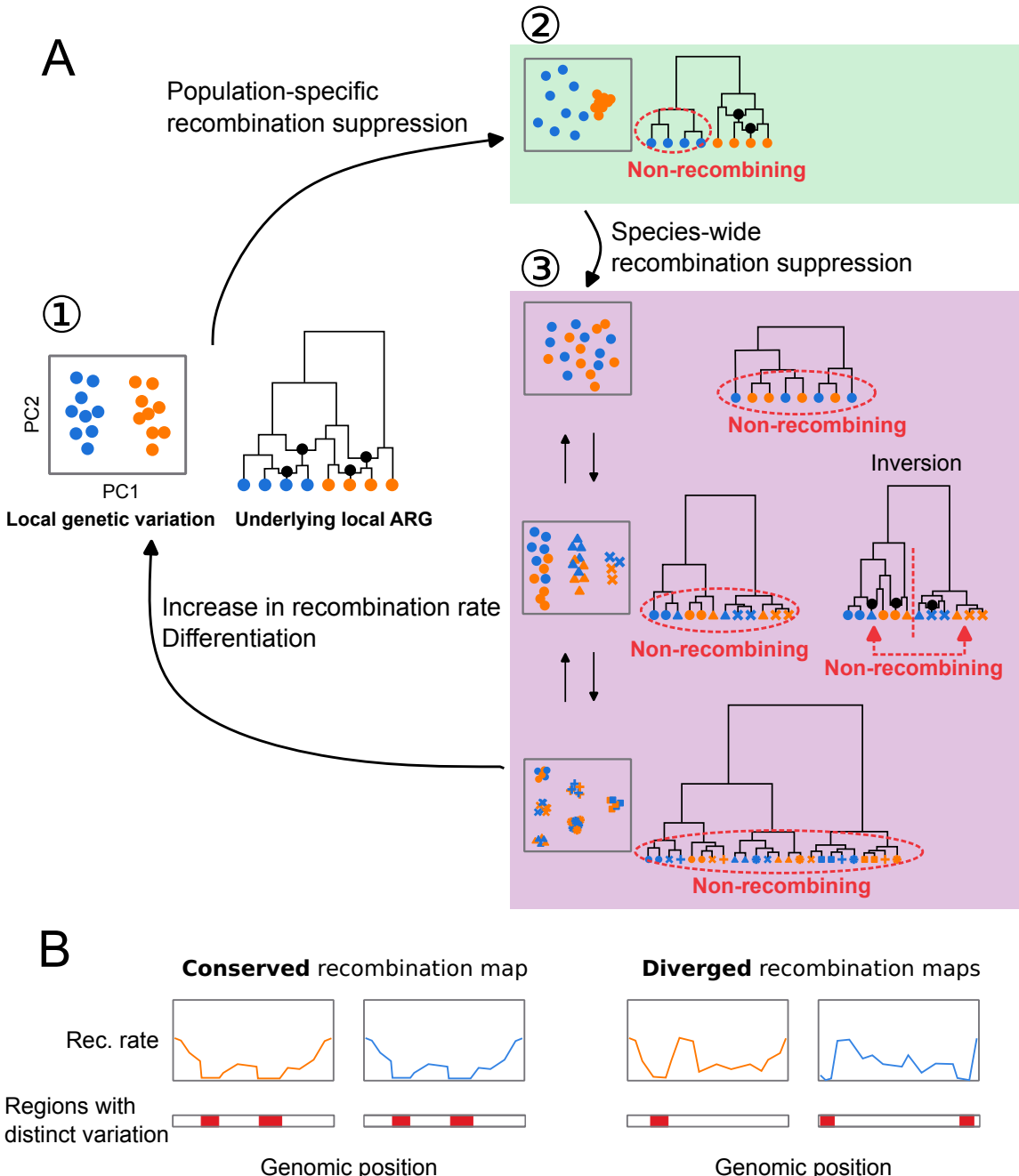


Figure 6: Evolutionary changes in local recombination rate influence evolution of local genetic variation. **A.** Local genetic variation is shown in hypothetical PCA plots. Their underlying genealogies are shown in simplified ancestral recombination graphs (ARGs), on which black dots represent ancestral recombination events contributing to the sampled sequences. Points in PCA depict diploid individuals, while those on the ARGs represent haploid sequences. Two colours of these points (blue and orange) indicate two populations. (1) Local genetic variation concordant to population structure. Genetic variation shows separation of individuals from two populations. ARG shows that recombination is suppressed in neither population. (2) Population-specific recombination suppression in the blue population. ARG shows that recombination is suppressed in the blue population. (3) Species-wide recombination suppression. Top: A case in which there are few mutations representing the basal splits of the underlying genealogy at species-wide low-recombining region. Middle: A case in which there are two haplotypic variants at the species-wide low-recombining region. If this is due to presence of an inversion (right ARG), recombination is suppressed between but not within the two clades representing two alleles. Bottom: A case in which there are three haplotypic variants at the species-wide low-recombining region. **B** Evolution of recombination map influences difference in genomic distributions of distinct patterns of genetic variation between species/populations.

349 Implications

350 Finally, we discuss technical and biological implications of our study. The technical implication
351 concerns interpretation of genome scans based on local genetic variation. A number of methods
352 based on local genetic variation have been used to detect loci involved in different kinds of
353 selective processes. For example, F_{ST} (differentiation), d_{XY} (divergence), and other population
354 parameters are inferred to detect genomic islands of speciation (Delmore et al., 2018; Hejase
355 et al., 2020; Huang et al., 2020; Malinsky et al., 2015). Reduced diversity (π) is a signature of
356 selection (Delmore et al., 2018; Irwin et al., 2018; Pracana et al., 2017), and by combining it
357 with variation among populations, loci associated with population-specific selection can be also
358 inferred (Yi et al., 2010). Targets of adaptive introgression have been identified by applying
359 statistics based on ABBA-BABA test, which is related to genetic variation (Peter, 2016, 2022),
360 in sliding windows (Kronforst et al., 2013; Martin et al., 2015; Patterson et al., 2012; Reich et
361 al., 2009). However, there are confounding factors that affect inference of these statistics. For
362 example, it has been shown that low diversity can cause elevation in some of these statistics
363 (Cruickshank & Hahn, 2014; Noor & Bennett, 2009). In addition to reduced diversity, this
364 study and others (Lotterhos, 2019; Renaut et al., 2013) show that reduced recombination rate
365 also causes distinct patterns of genetic variation which can lead to erroneous identification of
366 regions under influence of selective factors. Examining recombination rates at identified regions
367 and comparing them to other regions are necessary to avoid this. Furthermore, corroborating
368 methods based on different aspects of distinct patterns of variation, such as site frequency
369 spectrum (DeGiorgio et al., 2016; Fay & Wu, 2000; Tajima, 1989), LD (Sabeti et al., 2002,
370 2007; Voight et al., 2006), inferred genealogies (Hejase et al., 2020; Speidel et al., 2019; Stern
371 et al., 2019), local landscape of variation (Setter et al., 2020), and sites of mutations in genes
372 (Nei & Gojobori, 1986), as well as approaches with explicit simulation based on inferred
373 demography (Hager et al., 2022), may be informative.

374 The biological implication is about evolution of recombination rates and genetic variation
375 along the genome. Based on our findings of a link between these, we predict that organisms
376 with more conserved recombination landscape along the genome may have more conserved
377 genomic landscapes of distinct patterns of genetic variation (Fig. 6B). In other words, the

378 more conserved recombination maps are, the more correlated genomic distribution of distinct
379 genetic variation may be between species. In vertebrates including placental mammals (with
380 some exceptions), recombination landscape along the genome evolves fast due to continuous
381 turnovers of alleles of PRDM9 (the gene coding a protein that determines recombination hot
382 spots) and its target DNA sequences (Baudat et al., 2010; Myers et al., 2008). For instance,
383 in mammals that possess functional PRDM9, the genomic landscape of recombination rates is
384 distinct between and even within species (Kong et al., 2010; Spence & Song, 2019; Stevison
385 et al., 2016). Importantly, PRDM9 has been pseudogenised (Birtle & Ponting, 2006) or lost
386 (Baker et al., 2017) independently in multiple vertebrate lineages. This shifted the determinants
387 of recombination map from the PRDM9 allele and its target to genomic features such as CpG
388 islands and transcription start sites, stabilising the recombination landscape (Auton et al.,
389 2013; Baker et al., 2017; Singhal et al., 2015). Our results shown in birds, a group lacking
390 PRDM9 (Birtle & Ponting, 2006; Singhal et al., 2015), raises a question whether the evolution
391 of local recombination rates may play an even more important role in shaping local genetic
392 variation in organisms with functional PRDM9. Comparative studies using taxa with and
393 without functional PRDM9 will address this and may link the evolution of genomic landscape
394 of distinct patterns of genetic variation and (in)stability of recombination maps.

395 Materials and Methods

396 Empirical analyses

397 *de novo* genome assembly

398 A chromosome-level blackcap reference genome was *de novo* assembled within the Vertebrate
399 Genomes Project (VGP), following pipeline version 1.5 (Rhie et al., 2021). In brief, blood
400 of a female blackcap from the resident Tarifa population in Spain was collected in 100%
401 ethanol on ice and stored at -80 °C (NCBI BioSample accession SAMN12369542). The ethanol
402 supernatant was removed and the blood pellet was resuspended in Bionano Cell Buffer in
403 a 1:2 dilution. Ultra-long high molecular weight (HMW) DNA was isolated using Bionano
404 agarose plug method (Bionano Frozen Whole Nucleated Blood Stored in Ethanol – DNA

405 Isolation Guidelines (document number 30033)) using the Bionano Prep Blood and Cell Culture
406 DNA Isolation Kit. Four DNA extractions were performed yielding a total of 13.5 µg HMW
407 DNA. About 6 µg of DNA was sheared using a 26G blunt end needle (PacBio protocol PN
408 101-181-000 Version 05) to ~40 kb fragments. A large-insert PacBio library was prepared using
409 the Pacific Biosciences Express Template Prep Kit v1.0 following the manufacturer protocol.
410 The library was then size selected (>15 kb) using the Sage Science BluePippin Size-Selection
411 System. The library was then sequenced on 8 PacBio 1M v3 smrtcells on the Sequel instrument
412 with the sequencing kit 3.0 and 10 hours movie with 2 hours pre-extension time, yielding
413 77.51 Gb of data (~66.29X coverage) with N50 read length averaging around 22,927 bp. We
414 used the unfragmented HMW DNA to generate a linked-reads library on the 10X Genomics
415 Chromium (Genome Library Kit & Gel Bead Kit v2 , Genome Chip Kit v2 , i7 Multiplex
416 Kit PN-120262). We sequenced this 10X library on an Illumina Novaseq S4 150 bp PE lane
417 to ~60X coverage. Unfragmented HMW DNA was also used for Bionano Genomics optical
418 mapping. Briefly, DNA was labeled using the Bionano Prep Direct Label and Stain (DLS)
419 Protocol (30206E) and run on one Saphyr instrument chip flowcell. 136.31 Gb of data was
420 generated (N50 = 301.9kb with a label density = 16.91 labels/100kb). Optical maps were
421 assembled using Bionano Access (N50 = 27.48 Mb and total length = 1.41 Gb). Hi-C libraries
422 were generated by Arima Genomics and Dovetail Genomics and sequenced on HiSeq X at ~60X
423 coverage following the manufacturer's protocols. Proximally ligated DNA was produced using
424 the Arima-HiC kit v1 , sheared and size selected (200 – 600 bp) with SRI beads, and fragments
425 containing proximity-ligated DNA were enriched using streptavidin beads. A final Illumina
426 library was prepared using the KAPA Hyper Prep kit following the manufacturer guidelines.
427 FALCON v1.9.0 and FALCON unzip v1.0.6 were used to generate haplotype phased contigs,
428 and purge_haplotigs v1.0.3 was used to further sort out haplotypes (Guan et al., 2020). The
429 phased contigs were first scaffolded with 10X Genomics linked reads using scaff10X 4.1.0
430 software, followed with Bionano Genomics optical maps using Bionano Solve single enzyme
431 DLS 3.2.1, and Arima Genomics in-vitro cross-linked Hi-C maps using Salsa Hi-C 2.2 software
432 (Ghurye et al., 2019). Base call errors were polished with both PacBio long reads and Arrow
433 short reads to achieve above Q40 accuracy (no more than 1 error every 10,000 bp). Manual
434 curation was conducted using gEVAL software by the Sanger Institute Curation team (Howe

435 et al., 2021). Curation identified 33 autosomes and Z and W chromosomes (plus 1 unlocalised
436 W). Autosomes were named in decreasing order of size, and autosomes 1 through 30 and sex
437 chromosomes had counterparts in the commonly used VGP reference zebra finch assembly
438 (Sup. Table 2). The total length of the primary haplotype assembly was 1,066,786,587 bp,
439 with 99.14% assigned to chromosomes. The final 1.1 Gb assembly consisted of 601 contigs in
440 189 scaffolds, with a contig N50 of 7.4 Mb, and scaffold N50 of 73 Mb, indicating a high-quality
441 assembly that fulfills the VGP standard metrics.

442 **Whole-genome resequencing**

443 We resequenced 69 blackcap samples from various populations across the species distribution
444 range (Sup. Table 1) to complement an existing dataset of 110 blackcaps, 5 garden warblers,
445 and 3 African hill babblers that had been sequenced previously (Delmore et al., 2020b).
446 Blood samples from the additional 69 blackcaps were collected from the brachial vein and
447 stored in 100% ethanol. High molecular weight genomic DNA was extracted with a standard
448 salt extraction protocol or through the Nanobind CBB Big DNA Kit Beta following the
449 manufacturer's instructions. Libraries for short insert fragments between 300 and 500 bp were
450 prepared and were then sequenced for short paired-end reads on either Illumina NextSeq 500,
451 HiSeq 4000 or NovaSeq 5000 (Sup. Table 1).

452 We performed quality control of the reads with FastQC version 0.11.8 ([ht-
453 tps://www.bioinformatics.babraham.ac.uk/projects/fastqc/](https://www.bioinformatics.babraham.ac.uk/projects/fastqc/)). Reads from all samples
454 were mapped against the blackcap reference genome following an adjusted pipeline of **Genome
455 Analysis Toolkit** (GATK version 4.1.7.0, McKenna et al. (2010)) and **Picard** version 2.21.9
456 (<http://broadinstitute.github.io/picard/>). After resetting the base quality of adapter bases
457 in the sequenced reads to 2 with **Picard MarkIlluminaAdapters**, paired-end reads were
458 mapped to the reference using **BWA mem** (Li, 2013). To ensure that both unmapped mates and
459 secondary/supplementary reads were marked for duplicates, we ran **Picard MarkDuplicates**
460 for sorted reads with the default pixel distance of 100 for reads from Illumina NextSeq 500
461 or with a pixel distance of 2,500 for reads from HiSeq 4000 and NovaSeq 5000. Due to low
462 coverage, 10 samples (Sup. Table 1) were sequenced multiple times. Alignment files for these

463 samples (in BAM format) were merged with **Picard MergeSamFiles**. Per-sample quality
464 control of BAM files were performed using **QualiMap** version 2.2.1 (Okonechnikov et al., 2016),
465 **Picard CollectMultipleMetrics**, **CollectRawWgsMetrics** and **CollectWgsMetrics**; and
466 **MultiQC** version 1.8 (Ewels et al., 2016). We called bases at all positions per sample using
467 **GATK HaplotypeCaller**. We combined gVCF files of 189 individuals into ten evenly sized
468 subsets (to allow parallelisation of the following variant calling step) with **GATK CombineGVCFs**.
469 We genotyped SNPs and INDELs using **GATK GenotypeGVCFs**, and the 10 subsets were
470 concatenated using **Picard GatherVcfs** into one VCF file covering the entire genome. From
471 the VCF file, SNPs were selected (i.e. indels were excluded) using **GATK SelectVariants**,
472 after which we filtered SNPs with the following criteria: **QD < 2.5**; **FS > 45.0**; **SOR > 3.0**;
473 **MG < 40**; **MQRankSum < -12.5**; **ReadPosRankSum < -8.0**. We removed garden warblers
474 and African hill babblers from the multi-species VCF and kept only biallelic sites. We
475 estimated blackcap haplotypes using **SHAPEIT2** (r837) (Delaneau et al., 2013) with the
476 blackcap recombination map (Bascón-Cardozo et al., 2022a), yielding 142,083,056 SNPs.

477 Local PCA

478 To identify genomic regions with distinct patterns of genetic variation in blackcaps, we
479 performed local PCA in sliding genomic windows of 1,000 SNPs and summarised dissimilarity
480 of windows by multidimensional scaling using **lostrct** (Li & Ralph, 2019) in R version
481 3.5.3. First, we prepared a genotype and a haplotype table for each chromosome in which
482 rows and columns represented positions and individuals from the phased VCF file using
483 **BCFtools**. Specifically, genotypes were encoded 0, 1, and 2 for the reference allele homozygotes,
484 heterozygotes, and non-reference allele homozygotes in the genotype table, and 0 and 2 for the
485 reference and the non-reference allele in the haplotype table (encoding 0 and 1 instead of 0
486 and 2 in haplotype-based analysis gives the same results). Chromosomes shorter than 10 Mb
487 were concatenated to avoid misidentification of short chromosomal background as an outlier
488 region. Distance matrices of windows were computed based on the coordinates (PC1 and PC2)
489 of samples (individuals for genotype-based local PCA, and haplotype for haplotype-based
490 local PCA) within R using **lostruct**. Multidimensional scaling (MDS) was performed to
491 summarise similarities of local genetic variation patterns among windows into 20 axes (MDS1

492 through MDS20).

493 Using the **lostruct** output, we identified chromosomal intervals with distinct patterns
494 of genetic variation. In each chromosome, windows with MDS value apart from the mode
495 of the distribution by greater than 0.3 for any one of the 20 axes were defined as outlier
496 windows. This threshold was determined by visualising the distribution of MDS values in each
497 chromosome (Sup. Fig. 3). For each MDS axis, we defined genomic intervals with at least 10
498 outlier windows as “outlier regions” with distinct patterns of genetic variation. Overlapping
499 intervals across different MDS axes as well as intervals identified based on genotypes and
500 haplotypes were merged using **BEDtools**. To verify that the outliers show pattern of genetic
501 variation distinct from the whole-genome PCA, we performed PCA using all SNPs within each
502 outlier region using **PLINK** (Purcell et al., 2007). Genomic regions showing similar pattern to
503 the whole genome PCA were identified with visual inspection and discarded from the outliers.

504 To assess consistency between the pipelines using genotypes and haplotypes, we compared
505 MDS results of genotype- and haplotype-based **lostruct**. We calculated Euclidean distance of
506 windows from the centre of the 20 dimensional space to enable comparison of the same window
507 in genotype- and haplotype-based MDS. We measured this distance instead of comparing
508 the coordinates directly to account for possible rotations of MDS patterns between genotype-
509 and haplotype-based **lostruct**. Because dissimilarity of windows in terms of the pattern
510 of genetic variation was computed per chromosome, we calculated correlation of the above
511 distance between genotype- and haplotype-based methods per chromosome. The comparison
512 of genotype-based and haplotype-based **lostruct** is in Sup. Fig. 4.

513 To assess whether **lostruct** can identify outliers irrespective of presence/absence of
514 other outliers on the same chromosome as well as the chromosome length, we ran **lostruct**
515 treating either one part of a blackcap chromosome (“split chromosomes”) or multiple blackcap
516 chromosomes as a single chromosome (“joined chromosome”). If **lostruct** is robust to the
517 chromosomal background, it is expected that the same regions should be detected as outliers
518 with distinct patterns of genetic variation in both split and joined chromosomes compared
519 to per-chromosome results. We prepared four split chromosomes by splitting chromosomes
520 1 and 2 at the middle, and one joined chromosome by concatenating chromosomes 20, 21,

521 and 28. We performed `lостruct` analysis based both on genotype and haplotype and merged
522 the identified regions. The comparison of `lостruct` between using single chromosomes and
523 split/joined chromosomes is in Sup. Fig. 5.

524 **LD and recombination landscape**

525 To calculate LD around outlier regions, we first extracted SNPs within and 30% length outside
526 each outlier. We then thinned SNPs so that all neighbouring SNP positions were at least 10
527 kb away from each other. Linkage disequilibrium (LD) between all pairs of thinned SNPs was
528 calculated with `VCFTools` with the `--geno-r2`.

529 We inferred recombination landscape along blackcap chromosomes using `Pyrho` (Spence &
530 Song, 2019). `Pyrho` infers demography-aware recombination rates with a composite-likelihood
531 approach from SNPs data of unrelated samples making use of likelihood lookup tables generated
532 by simulations based on demography and sample size of each population. In all inferences,
533 we used demography of focal populations inferred in Delmore et al. (2020b). Before the
534 recombination inference, focal samples were filtered and singletons were removed. We ran
535 `Pyrho` with mutation rate of 4.6×10^{-9} per site per generation (Smeds et al., 2016), block
536 penalty of 20, and window size of 50 kb to infer population-level recombination landscape in
537 Azores, Cape Verde, continental resident, and medium-long distance migrants (represented
538 by medium distance south-west migrants). We computed mean recombination rate in 10 kb
539 sliding windows for each population.

540 To test association between local PCA outlier regions and low-recombinining regions, we
541 performed permutation tests. For this analysis we defined low-recombinining regions as genomic
542 intervals with recombination rate below 1 percentile for the entire genome. We counted
543 the number of overlaps in the observed data using `BEDtools`. For resampling, we shuffled
544 intervals corresponding to local PCA outlier regions within the genome 1,000 times and counted
545 the number of intervals overlapping the low-recombinining regions for each population using
546 `BEDtools`.

547 To characterise genotype-specific LD and recombination landscape at the five outlier
548 regions with three clusters of individuals in PCA, we applied `vcftools --geno-r2` and `Pyrho`

549 (Spence & Song, 2019) to our empirical data using each genotype (AA, AB, and BB in Sup.
550 Fig. 9) separately.

551 **Inversion breakpoints**

552 Three clusters of individuals observed in PCA with genotype-specific LD at two outlier regions
553 on chromosomes 12 and 30 were indicative of polymorphic inversion (Ma & Amos, 2012; Ruiz-
554 Arenas et al., 2019). To further characterise whether they represent polymorphic inversions,
555 we intended to locate breakpoints by two independent approaches.

556 **Soft-clip reads**

557 We attempted to identify positions where presence of soft-clipping of mapped reads is
558 associated with PCA-based genotype of the putative inversions. First, we extracted focal
559 regions around boundaries of the outliers (Sup. Table 4) from read mapping file of all
560 individuals using **SAMtools** (Danecek et al., 2021). Next, we identified soft clip reads in
561 each extracted region using **samextractclip** (Lindenbaum, 2015), and obtained reference
562 position corresponding to the position of soft clipping in mapped reads using a custom script.
563 At all extracted soft-clip positions, we counted the number of reads that switch to soft-clip
564 (“soft-clip depth”), as well as the depth of mapped reads, using **SAMtools**. At each of all
565 positions with at least one read supporting soft-clip switch, we calculated proportion of reads
566 with soft-clip switch relative to all mapped reads (depth of the position) for each individual
567 (“soft-clip proportion”). This resulted in “position-by-individual” matrix whose entry depicts
568 the proportion of soft-clip in all reads mapped at the focal position for the focal individual.
569 Using this matrix, we fit a linear model (soft-clip proportion \sim PCA – based genotype) in R at
570 each position treating genotypes AA, AB, and BB as 0, 1, and 2. Based on the significance of
571 genotype and R^2 of the linear models, we generated a list of 14 positions at which soft-clip
572 proportion was significantly associated with genotype of the putative inversions. We visualised
573 the distribution of the soft-clip proportion at these positions (Sup. Fig. 13) and selected six
574 positions for which the soft-clip proportion of BB was high enough and that of AB was around a
575 half of BB based on the assumption that soft clip reads covering an inversion breakpoint should
576 originate from haplotype B and non-soft clip reads should originate from haplotype A (Sup.

577 Table 5). To investigate whether some of these six positions represent inversion breakpoints,
578 we asked whether the soft-clipped segments of the reads have homologous sequences at the
579 other end of the outlier regions. We extracted soft-clipped segments of reads mapped at the
580 focal six positions in AB and BB individuals using a custom script, and re-mapped these
581 segments (instead of the entire reads) to the blackcap reference using **BWA mem**. We computed
582 the depth of mapped segments in each position using **SAMtools** (Sup. Table 5).

583 **10x linked read**

584 We used an independent set of blackcap individuals (hereafter “10x individuals”) whose
585 genomes were sequenced with the 10x linked-read technology (Delmore et al., 2023, NCBI
586 BioProject PRJEB65115). We genotyped the 10x individuals at the two putative inversion
587 loci (i.e. AA, AB, or BB) based on genotypes at diagnostic SNP positions. We started by
588 determining diagnostic SNP positions using our Illumina short read-based resequence data.
589 Because usable diagnostic SNP positions should have genotypes perfectly associated with
590 PCA-based genotype, we focused on positions at which F_{ST} was 1 between AA and BB,
591 and all AB were heterozygous, using **VCFtools** and **BCFtools**. We also recorded mapping
592 between an allele at the diagnostic positions and a genotype of the putative inversion (“A-
593 and B-diagnostic alleles”, e.g. G for haplotype A, T for haplotype B).

594 We then counted the number of sites with A- and B-diagnostic allele in each of 10x
595 samples. To convert coordinates of 10x assemblies to the reference coordinate, we mapped
596 the 10x pseudo-haplotted assemblies to the blackcap reference using **minimap2** (Li, 2018).
597 To determine the putative inversion genotype in the 10x individuals, we counted the number
598 of positions with A-diagnostic and B-diagnostic alleles for each 10x pseudo-haplotype, and
599 calculated the proportion of sites with A-diagnostic and B-diagnostic sites. In principle, an
600 AA and a BB individual respectively are expected to have proportion of 100% and 0% of
601 A-diagnostic sites in both of two pseudo-haplotypes, while an AB individual is expected to
602 have 100% of A-diagnostic sites in one pseudo-haplotype and 0% for the other. For genotyping,
603 we set the following three thresholds.

604 1. Missingness at the diagnostic positions is less than 10%, after removing positions with

605 non-unique `minimap2` mapping (i.e. at least 90% of all diagnostic positions should have
606 depth of 1x).

607 2. More than 90% of all diagnostic sites should agree per pseudo-haplotype.
608 3. The second criterion should be fulfilled for both pseudo-haplotypes of an individual.

609 We identified two BB individuals for each of the putative inversions on chromosomes 12
610 and 30. There were no AB individuals passing the above threshold, indicating 10x pseudo-
611 haplotyping is not accurate in separating two diverged non-recombining alleles at a long range
612 in an individual that has both. To identify breakpoints, we aligned the pseudo-haplotype
613 assemblies of these BB individuals as well as one AA individual for each putative inversion to
614 the blackcap reference using `Nucmer4` (Marçais et al., 2018), and generated dot plots (Sup.
615 Fig. 14).

616 **Sequence analysis at breakpoint of putative inversion on chromosome 12**

617 10x contigs of pseudo-haplotype B aligned next to the putative breakpoint position of
618 blackcap reference chromosome 12 had an un-aligned flanking sequence. To characterise the
619 DNA sequence of these flanking segments, we extracted the flanking sequences using `SAMtools`,
620 aligned the sequences to themselves using `minimap2`, and generated self-dot plots (Sup. Fig.
621 15), revealing presence of tandem repeats. To identify unit of tandem repeats within the
622 flanking sequences, we ran `TandemRepeatsFinder` against these extracted sequences, resulting
623 in four consensus unit sequences of 144 bp based on two contigs from two individuals. To
624 confirm that the four consensus sequences represent the same tandem repeat (because the unit
625 of identical tandem repeat can have different phases), we ran `BLASTn` (version 2.10.1, Altschul
626 et al., 1990) with each consensus as query against dimers of the consensus. To investigate
627 whether the tandem repeat found at the putative breakpoint of chromosome 12 in haplotype
628 B is present in chromosome 12 and other chromosomes of the reference and corresponding
629 position of haplotype A, we ran `BLASTn` with the 144 bp consensus of the tandem repeat unit as
630 the query against blackcap reference and a contig of an AA individual that spans the breakpoint
631 position, and counted how many copies were found in each reference chromosome/scaffold and
632 the 10x contig (Sup. Fig. 16).

633 **Selection in blackcaps**

634 To test for selection in different outlier regions and to compare them with the genome-wide
635 base line, we computed nucleotide diversity (π) and Tajima's D in 10 kb sliding windows
636 per population using **PopGenome** (Pfeifer et al., 2014) and **VCFtools** (Danecek et al., 2011)
637 respectively. The effects of the outlier regions on these statistics were tested using a linear
638 mixed effects model (**nlme**::**lme** (Pinheiro et al., 2021)) and a generalised linear mixed effects
639 model with a Gamma distribution (**lme4**::**glmer** (Bates et al., 2015)). To test for selection in
640 genes d_N/d_S were computed following the counting method by Nei & Gojobori (1986). Gene
641 annotation of the blackcap was obtained from Bascón-Cardozo et al. (2022b).

642 **Tandem repeats within and outside outlier regions**

643 To characterise correlation between outlier regions with distinct patterns of genetic variation
644 and tandem repeats, we identified tandem repeats in the reference genome and compared the
645 distribution of the tandem repeats with genomic regions with distinct patterns of genetic vari-
646 ation. First, **TandemRepeatsFinder** (Benson, 1999) was run on the blackcap reference genome
647 with the parameter set recommended on the documentation (**trf </path/to/fasta> 2 7 7**
648 **80 10 50 500 -f -d -m -h**). The output was formatted and summarised for visualisation
649 using custom scripts. Briefly, distribution of tandem repeats with a different unit size along
650 the genome was summarised in 100 kb sliding windows in blocks of repeat unit sizes of 10 bp
651 step (Sup. Fig. 26). Tandem repeats with the six longest repeat unit size were extracted per
652 chromosome, and copy number for each tandem repeat was counted (Sup. Fig. 27).

653 Next, we tested whether the number of tandem repeats with long repeat unit were
654 enriched in outlier regions at species-wide and population-specific low-recombinant regions. We
655 extracted tandem repeats with repeat unit size greater than or equal to 150 bp, and counted
656 the number of tandem repeats (instead of total copy number) within and outside outlier
657 regions. We performed Fisher's exact tests to test independence between the number of long
658 tandem repeats and the mode of recombination suppression (species-wide/population-specific)
659 (Sup. Table 7) using **fisher.test** function in R.

660 **Simulation**

661 **Validation of LD-based inference of recombination landscape using non-randomly**
662 **selected sample**

663 **Effects of recombination suppression model on recombination rate inference at**
664 **an inversion**

665 Three clusters of individuals observed in PCA at five outlier regions indicate presence of
666 distinct haplotypes. Polymorphic inversions are known to show this pattern due to suppression
667 of recombination between the normal and inverted alleles (Wellenreuther & Bernatchez, 2018).
668 To test whether some of the five outlier regions represent polymorphic inversions, we intended
669 to infer recombination rates using AA, AB, and BB individuals separately based on linkage
670 disequilibrium (LD) patterns. Before addressing this in blackcaps empirically, we assessed
671 how different types of recombination suppression at a haplotype block affect inference of
672 recombination landscape using a set of individuals with a certain combination of haplotypes.
673 To investigate the effect of a genotype-specific suppression of recombination on LD-based
674 inference of recombination rate, we simulated different modes of recombination suppression
675 using SLiM version 3.5 (Haller & Messer, 2019) under six scenarios listed in Sup. Table 6.
676 Specifically, we performed 1,000 replicates of forward-time simulations of two 500 kb-long
677 chromosomes with neutral mutation rate of 1×10^{-7} [per site per generation] and recombination
678 rate of 1×10^{-6} [per site per generation] in a population of 1,000 diploid individuals under
679 the Wright-Fisher model (We downscaled the population size and upscaled mutation rate to
680 minimise the time and computational resource for simulation). We introduced a mutation
681 (inversion marker) on one chromosome at 100 kb position at the 50th generation. We modelled
682 an inversion by suppressing recombination in an interval from 100 kb to 400 kb position if
683 the inversion marker site was heterozygous. We defined additional suppression according
684 to different scenarios (models 1-6). To allow for the inversion to remain in the population,
685 we applied negative frequency-dependent selection (fitness of inversion is $1 - (p_{inv} - 0.2)$ for
686 models 1-3 and $1 - (p_{inv} - 0.8)$ for models 4-6 where p_{inv} is the frequency of the inversion
687 allele). 1,000 generations after the inversion event, we recorded the mutations in all samples,
688 making a VCF file including all individuals. Although 1,000 generations is relatively short

689 given the population size of 1,000, the haplotype structure at the inversion locus was stable in
690 test runs of model-1 (inversion frequency of 0.2 without additional recombination suppression).
691 Based on the genotype at the marker, we randomly sampled 10 individuals for each inversion
692 genotype. **Pyrho** was run to estimate recombination rates using the sampled 10 individuals,
693 with the block penalty 50 and window size 50. The inferred recombination landscape is in
694 Sup. Fig. 11.

695 Species-wide reduction of recombination rate

696 To investigate how species-wide low-recombining regions affect patterns of local genetic variation
697 depicted in local PCA, we performed forward simulation with **SLiM** version 4.0.1 (Haller &
698 Messer, 2022). We simulated 100 replicates of two 500 kb-long chromosomes with neutral
699 mutation rate of 1×10^{-7} [per site per generation] and recombination rate of 1×10^{-6} [per
700 site per generation] except for an interval from 100 to 400 [kb] of the first chromosome
701 where recombination rate was set to 1×10^{-9} , which is 1/1000 of the normally recombining
702 chromosome. First, we ran a burn-in of 4,000 generations for an ancestral population of 1,000
703 diploids. After the burn-in, we made three populations of 1,000 diploids (pop1, pop2, and
704 pop3) split from the ancestral population. We sampled 50 individuals per population every 20
705 generations over 1,000 generations after the population split and recorded SNPs in VCF. For
706 each time point of each of 100 simulation replicates, we performed PCA with **PLINK**, using
707 SNPs either within 100 to 400 [kb] of the first chromosome (pop1-specific suppression) or the
708 normally recombining chromosome.

709 We investigated how reduced recombination rate affects representation of population
710 subdivision in local PCA. To evaluate whether the individuals from different populations were
711 distributed differently in local PCA at the low-recombining region, we performed Fasano-
712 Franceschini test (Fasano & Franceschini, 1987), which is a multi-dimensional extension of
713 Kolmogorov-Smirnov test, in three pairs of populations (pop1-pop2, pop1-pop3, pop2-pop3).
714 We counted the number of significant pairs of populations (0, 1, 2, or 3) for each time point of
715 each replicate. We compared between the low-recombining and normally recombining regions
716 the number of pairs of populations with distinct distribution in PCA (Sup. Fig. 24).

717 **Population-specific reduction of recombination rate**

718 To investigate how evolution of low-recombining regions in population(s) affect patterns of
719 local genetic variation depicted in local PCA, we performed forward simulation with **SLiM**
720 version 4.0.1. We simulated two 500kb-long chromosomes with neutral mutation rate and
721 recombination rate of 1×10^{-7} [per site per generation] and 1×10^{-6} [per site per generation].
722 First, we ran a burn-in of 4,000 generations for an ancestral population of 1,000 diploids. After
723 the burn-in, we made three populations of 1,000 diploids (pop1, pop2, and pop3) split from the
724 ancestral population, after which gene flow between all pairs of populations were set to 0.0025.
725 We introduced recombination suppression in pop1 from 100 to 400 [kb] of the first chromosome
726 in two scenarios. In the first scenario, recombination suppression was introduced at the same
727 time of the split. In the second scenario, recombination suppression was introduced 4,000
728 generations after the population split event, allowing the three populations to differentiate
729 before population-specific recombination suppression was introduced in pop1. We sampled 50
730 individuals per population every 20 generations over 1,000 generations after the introduction of
731 the population-specific suppression of recombination and recorded SNPs in VCF. For each time
732 point of each of 1,000 simulation replicates, we performed PCA with **PLINK**, using SNPs either
733 within 100 to 400 [kb] of the first chromosome (pop1-specific suppression) or the normally
734 recombining chromosome.

735 To characterise factors represented in the primary axes of distinct local PCA at population-
736 specific low-recombining regions, we performed one replicate of **SLiM** simulation with the same
737 scenarios of models 1 and 2 recording the full ancestry and mutations in tree sequence, with an
738 increased duration of burn-in (40,000 generations) to make sure that all lineages at sampling
739 time coalesce. We loaded the tree sequence with mutations in **tskit** (Kelleher et al., 2018)
740 and sampled 50 diploids per population, and saved SNPs in VCF. Using the VCF files for
741 each time point for each model, we performed PCA using **PLINK** at the population-specific
742 low-recombining region, and determined one time point per model showing typical spread
743 of individuals from the low-recombining population in PCA (Sup. Fig. 20A, E). For these
744 PCAs we identified 5% SNPs with the highest loadings to the first two PC axes. We analysed
745 these mutations on the underlying genealogies using **tskit**. Specifically, we investigated

746 whether mutations originating from the low-recombining population were enriched in the
747 high-loading mutations (Sup. Fig. 20C, G) with a χ^2 test. We also assessed whether multiple
748 mutations originating in the low-recombining population occurring on the same genealogical
749 branches (i.e. mutations on the same ancestral haplotypes) were enriched in the high-loading
750 mutations (Sup. Fig. 20D, H). For this, we compared the number of mutations sharing
751 the same genealogical branches among the high-loading mutations originating from the low-
752 recombining population and the same number of randomly-selected mutations originating from
753 the low-recombining population by a Kolmogorov-Smirnov test.

754 Effects of linked selection on local PCA

755 Background selection

756 To investigate the linked effect of purifying selection at low-recombining regions (back-
757 ground selection) on patterns of local genetic variation represented in local PCA, we performed
758 forward simulation with **SLiM** version 4.0.1. We simulated a species-wide low-recombining
759 region in three populations as described above, except we changed the distribution of fitness
760 effect of mutations with three different ratios between neutral (“n”, $s = 0$) and deleterious
761 (“d”, $s = -0.05$ and $h = 0.5$) mutations of $n/(n + d) = 0, 0.25, 0.5, 0.75$. To evaluate whether
762 individuals from different populations were distributed differently in the local PCA at the
763 low-recombining region, we performed Fasano-Franceschini test between three pairs of popu-
764 lations (pop1-pop2, pop1-pop3, pop2-pop3). We counted the number of significant pairs of
765 populations (0, 1, 2, or 3) for each sampled time point of each replicate (out of 100) for each
766 DFE (Sup. Fig. 24).

767 Positive selection

768 To investigate the linked effect of positive selection at low-recombining regions on patterns
769 of local genetic variation represented in local PCA, we performed forward simulation with **SLiM**
770 version 4.0.1 under four scenarios: population-specific sweep and sweep before populations
771 split, with and without reduced local recombination rate. We simulated 10 replicates of one
772 500 kb-long chromosome with neutral mutation rate of 1×10^{-7} [per site per generation]

773 and recombination rate of 1×10^{-6} [per site per generation]. In scenarios with reduced
774 recombination rate, we introduced a reduced recombination rate within an interval from 100
775 to 400 [kb] of the chromosome where recombination rate was set to 1×10^{-9} , which is 1/1000
776 of the normally recombining regions. For all scenarios, we ran a burn-in of 4,000 generations
777 for an ancestral population of 1,000 diploids. In the scenarios with population-specific sweep,
778 we made three populations of 1,000 diploids (pop1, pop2, and pop3) split from the ancestral
779 population at the 4000-th generation. We introduced a strongly beneficial mutation ($s = 1$
780 and $h = 0.5$) in the middle of a chromosome of one randomly selected sample of the first
781 population at the 100-th generation after the populations split. In the scenarios with sweep
782 before split, we introduced a strongly beneficial mutation ($s = 1$ and $h = 0.5$) in the middle of
783 the chromosome of one randomly selected sample of the ancestral population, and made the
784 three populations of 1,000 diploids split at the 100-th generation after the introduction of the
785 beneficial mutation. We sampled 100 diploid individuals per population every 20 generations
786 since the introduction of the beneficial mutation (scenarios of population-specific sweep) or
787 the split (scenarios of ancestral sweep) and recorded the SNPs in VCF format. We performed
788 PCA using PLINK.

789 Acknowledgment

790 This work was supported by the Max Planck Society (Max Planck Research Group grant
791 MFFALIMN0001 to ML), the DFG (project Z02 and Nav05 within SFB 1372 – Magnetore-
792 ception and Navigation in Vertebrates to ML), and DFG Research Infrastructure NGS_CC
793 (project 407495230) as part of the Next Generation Sequencing Competence Network (project
794 423957469). AR was supported by the Intramural Research Program of the NHGRI, NIH
795 (1ZIAHG200398). We thank Britta Meyer, Tianhao Zhao, Hanna Koch, Conny Burghardt,
796 and Sven Künzel for DNA extraction, library preparation, and/or sequencing. We are grateful
797 to Julien Dutheil, Diethard Tautz, Linda Odenthal-Hesse, Tobias Kaiser, Carolina Peralta,
798 and Matthias Weissensteiner for constructive discussion. We are grateful to Thord Fransson,
799 Christos Barboutis, Zura Javakhishvili, Martim Melo, Álvaro Ramírez, and Helena Batalha
800 for providing us with samples. Permits were provided to JCI for samples collected on Cape

801 Verde (Ministerio do Ambiente - Habitacao e Ordenamento do Territorio, 18/CITES/DNA,
802 17 Dec 2015), Canary Islands (Ref.: 2012/0710), Madeira (Ref.: 02/2016), and the Azores
803 (Instituto da Conservacao da Natureza e da Biodiversidade, 171/2008, 31 Mar 2009); to JP-T
804 for samples collected on Mallorca (CAP 64/2009); to Thord Fransson for samples collected on
805 Crete (6Υ0Ξ4653Π8-ΥΓ5 issued by the Hellenic Ministry of Environment and Energy), and to
806 Zura Javakhishvili for samples collected in Georgia (889-0-2-202303291450 by the Ministry of
807 Environment and Agriculture of Georgia).

808 Data availability

809 The primary and alternate haplotype assemblies of the blackcap reference genome can be found
810 under NCBI BioProject PRJNA558064 (accession GCA_009819655.1) and PRJNA558065
811 (accession GCA_009819715.1). Raw Illumina reads for the resequencing data can be accessed
812 under NCBI BioProject PRJEB66075 (SRA accession ERP151147). Processed data and scripts
813 for analysis and simulation are found in Zenodo (<https://doi.org/10.5281/zenodo.8358874>).

814 Conflict of interest

815 The authors declare no conflict of interest.

816 Author contributions

817 JI and ML designed the study. Reference genome was generated by JF, AR, JM, BH, WC,
818 JC, KH, MU, OF, and EDJ. JP-T and JCI collected samples for resequencing. AB performed
819 read mapping, variant calling, and data filtration. KB-C inferred recombination maps. JI
820 conducted haplotype inference, population genomics analyses, simulations, sequence analyses,
821 statistical modelling, and data visualisation. JI and ML wrote the manuscript with inputs
822 from other authors.

823 References

824 Altschul, S. F., Gish, W., Miller, W., Myers, E. W., & Lipman, D. J. (1990). Basic local
825 alignment search tool. *Journal of Molecular Biology*, 215(3), 403–410. [https://doi.org/10.1016/S0022-2836\(05\)80360-2](https://doi.org/10.1016/S0022-2836(05)80360-2)

826

827 Auton, A., Li, Y. R., Kidd, J., Oliveira, K., Nadel, J., Holloway, J. K., Hayward, J. J., Cohen,
828 P. E., Greally, J. M., Wang, J., Bustamante, C. D., & Boyko, A. R. (2013). Genetic
829 Recombination Is Targeted towards Gene Promoter Regions in Dogs. *PLOS Genetics*,
830 9(12), e1003984. <https://doi.org/10.1371/journal.pgen.1003984>

831 Baker, Z., Schumer, M., Haba, Y., Bashkirova, L., Holland, C., Rosenthal, G. G., & Przeworski,
832 M. (2017). Repeated losses of PRDM9-directed recombination despite the conservation of
833 PRDM9 across vertebrates. *eLife*, 6, e24133. <https://doi.org/10.7554/eLife.24133>

834 Barton, N. H., & Etheridge, A. M. (2004). The Effect of Selection on Genealogies. *Genetics*,
835 166(2), 1115–1131. <https://doi.org/10.1093/genetics/166.2.1115>

836 Bascón-Cardozo, K., Bours, A., Ishigohoka, J., Odenthal-Hesse, L., & Liedvogel, M. (2022a).
837 *Historical recombination maps diverge between Eurasian blackcap populations with dis-*
838 *distinct migratory strategies* [Preprint]. Authorea. <https://doi.org/10.22541/au.166790167.72861799/v1>

839

840 Bascón-Cardozo, K., Bours, A., Manthey, G., Pruijscher, P., Durieux, G., Dutheil, J., Odenthal-
841 Hesse, L., & Liedvogel, M. (2022b). *Fine-scale map reveals highly variable recombination*
842 *rates associated with genomic features in the European blackcap* [Preprint]. Authorea.
843 <https://doi.org/10.22541/au.165423614.49331155/v1>

844 Bates, D., Mächler, M., Bolker, B., & Walker, S. (2015). Fitting Linear Mixed-Effects Models
845 Using lme4. *Journal of Statistical Software*, 67(1), 1–48. <https://doi.org/10.18637/jss.v067.i01>

846

847 Baudat, F., Buard, J., Grey, C., Fledel-Alon, A., Ober, C., Przeworski, M., Coop, G., & Massy,
848 B. de. (2010). PRDM9 Is a Major Determinant of Meiotic Recombination Hotspots in
849 Humans and Mice. *Science*, 327(5967), 836–840. <https://doi.org/10.1126/science.1183439>

850 Benson, G. (1999). Tandem repeats finder: A program to analyze DNA sequences. *Nucleic
851 Acids Research*, 27(2), 573–580. <https://doi.org/10.1093/nar/27.2.573>

852 Berthold, P. (1988). Evolutionary aspects of migratory behavior in European warblers. *Journal
853 of Evolutionary Biology*, 1(3), 195–209. <https://doi.org/https://doi.org/10.1046/j.1420-9101.1998.1030195.x>

854

855 Berthold, P. (1991). Genetic control of migratory behaviour in birds. *Trends in Ecology and
856 Evolution*, 6(8), 254–257. [https://doi.org/10.1016/0169-5347\(91\)90072-6](https://doi.org/10.1016/0169-5347(91)90072-6)

857 Bhatia, G., Patterson, N., Sankararaman, S., & Price, A. L. (2013). Estimating and interpreting
858 FST: The impact of rare variants. *Genome Research*, 23(9), 1514–1521. <https://doi.org/10.1101/gr.154831.113>

859

860 Birtle, Z., & Ponting, C. P. (2006). Meisetz and the birth of the KRAB motif. *Bioinformatics*,

861 22(23), 2841–2845. <https://doi.org/10.1093/bioinformatics/btl498>

862 Burri, R. (2017). Interpreting differentiation landscapes in the light of long-term linked selection.
863 *Evolution Letters*, 1(3), 118–131. <https://doi.org/https://doi.org/10.1002/evl3.14>

864 Burri, R., Nater, A., Kawakami, T., Mugal, C. F., Olason, P. I., Smeds, L., Suh, A., Dutoit,
865 L., Bureš, S., Garamszegi, L. Z., Hogner, S., Moreno, J., Qvarnström, A., Ružić, M.,
866 Sæther, S.-A., Sætre, G.-P., Török, J., & Ellegren, H. (2015). Linked selection and
867 recombination rate variation drive the evolution of the genomic landscape of differentiation
868 across the speciation continuum of Ficedula flycatchers. *Genome Research*, 25(11), 1656–
869 1665. <https://doi.org/10.1101/gr.196485.115>

870 Cao, Y., Li, L., Xu, M., Feng, Z., Sun, X., Lu, J., Xu, Y., Du, P., Wang, T., Hu, R., Ye,
871 Z., Shi, L., Tang, X., Yan, L., Gao, Z., Chen, G., Zhang, Y., Chen, L., Ning, G., et al.
872 (2020). The ChinaMAP analytics of deep whole genome sequences in 10,588 individuals.
873 *Cell Research*, 30(9), 717–731. <https://doi.org/10.1038/s41422-020-0322-9>

874 Cruickshank, T. E., & Hahn, M. W. (2014). Reanalysis suggests that genomic islands of
875 speciation are due to reduced diversity, not reduced gene flow. *Molecular Ecology*, 23(13),
876 3133–3157. <https://doi.org/https://doi.org/10.1111/mec.12796>

877 Danecek, P., Auton, A., Abecasis, G., Albers, C. A., Banks, E., DePristo, M. A., Handsaker,
878 R. E., Lunter, G., Marth, G. T., Sherry, S. T., McVean, G., Durbin, R., & 1000 Genomes
879 Project Analysis Group. (2011). The variant call format and VCFtools. *Bioinformatics*,
880 27(15), 2156–2158. <https://doi.org/10.1093/bioinformatics/btr330>

881 Danecek, P., Bonfield, J. K., Liddle, J., Marshall, J., Ohan, V., Pollard, M. O., Whitwham,
882 A., Keane, T., McCarthy, S. A., Davies, R. M., & Li, H. (2021). Twelve years of SAMtools
883 and BCFtools. *GigaScience*, 10(giab008). <https://doi.org/10.1093/gigascience/giab008>

884 DeGiorgio, M., Huber, C. D., Hubisz, M. J., Hellmann, I., & Nielsen, R. (2016). SweepFinder2:
885 Increased sensitivity, robustness and flexibility. *Bioinformatics*, 32(12), 1895–1897. <https://doi.org/10.1093/bioinformatics/btw051>

886 Delaneau, O., Zagury, J.-F., & Marchini, J. (2013). Improved whole-chromosome phasing for
887 disease and population genetic studies. *Nature Methods*, 10(1), 5–6. <https://doi.org/10.1038/nmeth.2307>

888 Delmore, K., Doren, B. M. V., Ullrich, K., Curk, T., Jeugd, H. P. van der, & Liedvogel, M.
889 (2023). *Structural genomic variation and migratory behavior in wild songbirds* [Preprint].
890 bioRxiv. <https://doi.org/10.1101/2023.04.24.538030>

891 Delmore, K. E., Lugo Ramos, J. S., Van Doren, B. M., Lundberg, M., Bensch, S., Irwin, D. E.,
892 & Liedvogel, M. (2018). Comparative analysis examining patterns of genomic differentiation
893 across multiple episodes of population divergence in birds. *Evolution Letters*, 2(2), 76–87.
894 <https://doi.org/10.1002/evl3.46>

895 Delmore, K. E., Van Doren, B. M., Conway, G. J., Curk, T., Garrido-Garduño, T., Germain,
896 R. R., Hasselmann, T., Hiemer, D., Jeugd, H. P. van der, Justen, H., Lugo Ramos, J. S.,
897 Maggini, I., Meyer, B. S., Phillips, R. J., Remisiewicz, M., Roberts, G. C. M., Sheldon,
898 B. C., Vogl, W., & Liedvogel, M. (2020a). Individual variability and versatility in an
899 eco-evolutionary model of avian migration. *Proceedings of the Royal Society B: Biological
900 Sciences*, 287(1948), 20200346. <https://doi.org/10.1098/rspb.2020.0346>

902 *Sciences*, 287(1938), 20201339. <https://doi.org/10.1098/rspb.2020.1339>

903 Delmore, K., Illera, J. C., Pérez-Tris, J., Segelbacher, G., Ramos, J. S., Durieux, G., Ishigohoka, J., & Liedvogel, M. (2020b). The evolutionary history and genomics of european blackcap migration. *eLife*, 9, e54462. <https://doi.org/10.7554/eLife.54462>

906 Dutheil, J. Y., Ganapathy, G., Hobolth, A., Mailund, T., Uyenoyama, M. K., & Schierup, M. H. (2009). Ancestral Population Genomics: The Coalescent Hidden Markov Model Approach. *Genetics*, 183(1), 259–274. <https://doi.org/10.1534/genetics.109.103010>

909 Ewels, P., Magnusson, M., Lundin, S., & Käller, M. (2016). MultiQC: Summarize analysis results for multiple tools and samples in a single report. *Bioinformatics*, 32(19), 3047–3048. <https://doi.org/10.1093/bioinformatics/btw354>

912 Faria, R., Johannesson, K., Butlin, R. K., & Westram, A. M. (2019). Evolving Inversions. *Trends in Ecology & Evolution*, 34(3), 239–248. <https://doi.org/10.1016/j.tree.2018.12.005>

914 Fasano, G., & Franceschini, A. (1987). A multidimensional version of the Kolmogorov–Smirnov test. *Monthly Notices of the Royal Astronomical Society*, 225(1), 155–170. <https://doi.org/10.1093/mnras/225.1.155>

917 Fay, J. C., & Wu, C.-I. (2000). Hitchhiking Under Positive Darwinian Selection. *Genetics*, 155(3), 1405–1413. <https://doi.org/10.1093/genetics/155.3.1405>

919 Fedorova, S. A., Reidla, M., Metspalu, E., Metspalu, M., Roots, S., Tambets, K., Trofimova, N., Zhdanov, S. I., Kashani, B. H., Olivieri, A., Voevoda, M. I., Osipova, L. P., Platonov, F. A., Tomsky, M. I., Khusnutdinova, E. K., Torroni, A., & Villems, R. (2013). Autosomal and uniparental portraits of the native populations of Sakha (Yakutia): Implications for the peopling of Northeast Eurasia. *BMC Evolutionary Biology*, 13(1), 127. <https://doi.org/10.1186/1471-2148-13-127>

925 Ghurye, J., Rhie, A., Walenz, B. P., Schmitt, A., Selvaraj, S., Pop, M., Phillippy, A. M., & Koren, S. (2019). Integrating Hi-C links with assembly graphs for chromosome-scale assembly. *PLOS Computational Biology*, 15(8), e1007273. <https://doi.org/10.1371/journal.pcbi.1007273>

929 Guan, D., McCarthy, S. A., Wood, J., Howe, K., Wang, Y., & Durbin, R. (2020). Identifying and removing haplotypic duplication in primary genome assemblies. *Bioinformatics*, 36(9), 2896–2898. <https://doi.org/10.1093/bioinformatics/btaa025>

932 Guerrero, R. F., Rousset, F., & Kirkpatrick, M. (2012). Coalescent patterns for chromosomal inversions in divergent populations. *Philosophical Transactions of the Royal Society B: Biological Sciences*, 367(1587), 430–438. <https://doi.org/10.1098/rstb.2011.0246>

935 Hager, E. R., Harringmeyer, O. S., Wooldridge, T. B., Theingi, S., Gable, J. T., McFadden, S., Neugeboren, B., Turner, K. M., Jensen, J. D., & Hoekstra, H. E. (2022). A chromosomal inversion contributes to divergence in multiple traits between deer mouse ecotypes. *Science*, 377(6604), 399–405. <https://doi.org/10.1126/science.abg0718>

939 Haller, B. C., & Messer, P. W. (2019). SLiM 3: Forward Genetic Simulations Beyond the Wright–Fisher Model. *Molecular Biology and Evolution*, 36(3), 632–637. <https://doi.org/10.1093/molbev/msy228>

942 Haller, B. C., & Messer, P. W. (2022). SLiM 4: Multispecies Eco-Evolutionary Modeling. *The*
943 *American Naturalist*, E000–E000. <https://doi.org/10.1086/723601>

944 Hejase, H. A., Salman-Minkov, A., Campagna, L., Hubisz, M. J., Lovette, I. J., Gronau, I.,
945 & Siepel, A. (2020). Genomic islands of differentiation in a rapid avian radiation have
946 been driven by recent selective sweeps. *Proceedings of the National Academy of Sciences*,
947 117(48), 30554–30565. <https://doi.org/10.1073/pnas.2015987117>

948 Helbig, A. J. (1991). Inheritance of migratory direction in a bird species: A cross-breeding
949 experiment with SE- and SW-migrating blackcaps (*Sylvia atricapilla*). *Behavioral Ecology*
950 and *Sociobiology*, 28(1), 9–12. <https://doi.org/10.1007/BF00172133>

951 Howe, K., Chow, W., Collins, J., Pelan, S., Pointon, D.-L., Sims, Y., Torrance, J., Tracey,
952 A., & Wood, J. (2021). Significantly improving the quality of genome assemblies through
953 curation. *GigaScience*, 10(1), giaa153. <https://doi.org/10.1093/gigascience/giaa153>

954 Huang, K., Andrew, R. L., Owens, G. L., Ostevik, K. L., & Rieseberg, L. H. (2020). Multiple
955 chromosomal inversions contribute to adaptive divergence of a dune sunflower ecotype.
956 *Molecular Ecology*, 29(14), 2535–2549. <https://doi.org/https://doi.org/10.1111/mec.15428>

957 Hudson, R. R. (1983). Properties of a neutral allele model with intragenic recombination.
958 *Theoretical Population Biology*, 23(2), 183–201. [https://doi.org/10.1016/0040-5809\(83\)90013-8](https://doi.org/10.1016/0040-5809(83)90013-8)

959 Irwin, D. E., Milá, B., Toews, D. P. L., Brelsford, A., Kenyon, H. L., Porter, A. N., Grossen,
960 C., Delmore, K. E., Alcaide, M., & Irwin, J. H. (2018). A comparison of genomic islands of
961 differentiation across three young avian species pairs. *Molecular Ecology*, 27(23), 4839–4855.
962 <https://doi.org/https://doi.org/10.1111/mec.14858>

963 Kelleher, J., Thornton, K. R., Ashander, J., & Ralph, P. L. (2018). Efficient pedigree recording
964 for fast population genetics simulation. *PLOS Computational Biology*, 14(11), e1006581.
965 <https://doi.org/10.1371/journal.pcbi.1006581>

966 Kong, A., Thorleifsson, G., Gudbjartsson, D. F., Masson, G., Sigurdsson, A., Jonasdottir, A.,
967 Walters, G. B., Jonasdottir, A., Gylfason, A., Kristinsson, K. T., Gudjonsson, S. A., Frigge,
968 M. L., Helgason, A., Thorsteinsdottir, U., & Stefansson, K. (2010). Fine-scale recombination
969 rate differences between sexes, populations and individuals. *Nature*, 467(7319), 1099–1103.
970 <https://doi.org/10.1038/nature09525>

971 Kronforst, M. R., Hansen, M. E. B., Crawford, N. G., Gallant, J. R., Zhang, W., Kulathinal,
972 R. J., Kapan, D. D., & Mullen, S. P. (2013). Hybridization Reveals the Evolving Genomic
973 Architecture of Speciation. *Cell Reports*, 5(3), 666–677. <https://doi.org/10.1016/j.celrep.9742013.09.042>

975 Li, H. (2013). Aligning sequence reads, clone sequences and assembly contigs with BWA-MEM
976 [Preprint]. arXiv. <https://doi.org/https://doi.org/10.48550/arXiv.1303.3997>

977 Li, H. (2018). Minimap2: Pairwise alignment for nucleotide sequences. *Bioinformatics*, 34(18),
978 3094–3100. <https://doi.org/10.1093/bioinformatics/bty191>

979 Li, H., & Ralph, P. (2019). Local PCA Shows How the Effect of Population Structure Differs
980 Along the Genome. *Genetics*, 211(1), 289–304. <https://doi.org/10.1534/genetics.118.301747>

982 Lindenbaum, P. (2015). *JVarkit: Java-based utilities for Bioinformatics*. <https://doi.org/10.6084/m9.figshare.1425030.v1>

984 Lotterhos, K. E. (2019). The Effect of Neutral Recombination Variation on Genome Scans for
985 Selection. *G3 GenesGenomesGenetics*, 9(6), 1851–1867. <https://doi.org/10.1534/g3.119.400088>

987 Ma, J., & Amos, C. I. (2012). Investigation of Inversion Polymorphisms in the Human Genome
988 Using Principal Components Analysis. *PLOS ONE*, 7(7), e40224. <https://doi.org/10.1371/journal.pone.0040224>

990 Malinsky, M., Challis, R. J., Tyers, A. M., Schiffels, S., Terai, Y., Ngatunga, B. P., Miska,
991 E. A., Durbin, R., Genner, M. J., & Turner, G. F. (2015). Genomic islands of speciation
992 separate cichlid ecomorphs in an East African crater lake. *Science*, 350(6267), 1493–1498.
993 <https://doi.org/10.1126/science.aac9927>

994 Marçais, G., Delcher, A. L., Phillippy, A. M., Coston, R., Salzberg, S. L., & Zimin, A. (2018).
995 MUMmer4: A fast and versatile genome alignment system. *PLOS Computational Biology*,
996 14(1), e1005944. <https://doi.org/10.1371/journal.pcbi.1005944>

997 Martin, S. H., Davey, J. W., & Jiggins, C. D. (2015). Evaluating the Use of ABBA–BABA
998 Statistics to Locate Introgressed Loci. *Molecular Biology and Evolution*, 32(1), 244–257.
999 <https://doi.org/10.1093/molbev/msu269>

1000 Martin, S. H., Davey, J. W., Salazar, C., & Jiggins, C. D. (2019). Recombination rate variation
1001 shapes barriers to introgression across butterfly genomes. *PLoS Biology*, 17(2), 1–28.
1002 <https://doi.org/10.1371/journal.pbio.2006288>

1003 Martin, S. H., & Van Belleghem, S. M. (2017). Exploring Evolutionary Relationships Across
1004 the Genome Using Topology Weighting. *Genetics*, 206(1), 429–438. <https://doi.org/10.1534/genetics.116.194720>

1006 McKenna, A., Hanna, M., Banks, E., Sivachenko, A., Cibulskis, K., Kernytsky, A., Garimella,
1007 K., Altshuler, D., Gabriel, S., Daly, M., & DePristo, M. A. (2010). The Genome Analysis
1008 Toolkit: A MapReduce framework for analyzing next-generation DNA sequencing data.
1009 *Genome Research*, 20(9), 1297–1303. <https://doi.org/10.1101/gr.107524.110>

1010 McVean, G. (2009). A Genealogical Interpretation of Principal Components Analysis. *PLOS
1011 Genetics*, 5(10), e1000686. <https://doi.org/10.1371/journal.pgen.1000686>

1012 McVean, G. A., & Cardin, N. J. (2005). Approximating the coalescent with recombination.
1013 *Philosophical Transactions of the Royal Society B: Biological Sciences*, 360(1459), 1387–1393.
1014 <https://doi.org/10.1098/rstb.2005.1673>

1015 Merot, C., Berdan, E. L., Cayuela, H., Djambazian, H., Ferchaud, A.-L., Laporte, M.,
1016 Normandeau, E., Ragoussis, J., Wellenreuther, M., & Bernatchez, L. (2021). Locally
1017 Adaptive Inversions Modulate Genetic Variation at Different Geographic Scales in a Seaweed
1018 Fly. *Molecular Biology and Evolution*, 38(9), 3953–3971. <https://doi.org/10.1093/molbev/msab143>

1020 Myers, S., Freeman, C., Auton, A., Donnelly, P., & McVean, G. (2008). A common sequence
1021 motif associated with recombination hot spots and genome instability in humans. *Nature
1022 Genetics*, 40(9), 1124–1129. <https://doi.org/10.1038/ng.213>

1023 Nei, M., & Gojobori, T. (1986). Simple methods for estimating the numbers of synonymous and
1024 nonsynonymous nucleotide substitutions. *Molecular Biology and Evolution*, 3(5), 418–426.
1025 <https://doi.org/10.1093/oxfordjournals.molbev.a040410>

1026 Nielsen, R. (2005). Molecular Signatures of Natural Selection. *Annual Review of Genetics*,
1027 39(1), 197–218. <https://doi.org/10.1146/annurev.genet.39.073003.112420>

1028 Noor, M., & Bennett, S. (2009). Islands of speciation or mirages in the desert? Examining the
1029 role of restricted recombination in maintaining species. *Heredity*, 103, 439–444.

1030 Okonechnikov, K., Conesa, A., & García-Alcalde, F. (2016). Qualimap 2: Advanced multi-
1031 sample quality control for high-throughput sequencing data. *Bioinformatics*, 32(2), 292–294.
1032 <https://doi.org/10.1093/bioinformatics/btv566>

1033 Pamilo, P., & Nei, M. (1988). Relationships between gene trees and species trees. *Molecular
1034 Biology and Evolution*, 5(5), 568–583. [https://doi.org/10.1093/oxfordjournals.molbev.a040517](https://doi.org/10.1093/oxfordjournals.molbev.
1035 a040517)

1036 Patterson, N., Moorjani, P., Luo, Y., Mallick, S., Rohland, N., Zhan, Y., Genschoreck, T.,
1037 Webster, T., & Reich, D. (2012). Ancient Admixture in Human History. *Genetics*, 192(3),
1038 1065–1093. <https://doi.org/10.1534/genetics.112.145037>

1039 Patterson, N., Price, A. L., & Reich, D. (2006). Population Structure and Eigenanalysis.
1040 *PLOS Genetics*, 2(12), e190. <https://doi.org/10.1371/journal.pgen.0020190>

1041 Peter, B. M. (2016). Admixture, Population Structure, and F-Statistics. *Genetics*, 202(4),
1042 1485–1501. <https://doi.org/10.1534/genetics.115.183913>

1043 Peter, B. M. (2022). A geometric relationship of F2, F3 and F4-statistics with principal
1044 component analysis. *Philosophical Transactions of the Royal Society B: Biological Sciences*,
1045 377(1852), 20200413. <https://doi.org/10.1098/rstb.2020.0413>

1046 Pfeifer, B., Wittelsbuerger, U., Ramos-Onsins, S. E., & Lercher, M. J. (2014). PopGenome:
1047 An Efficient Swiss Army Knife for Population Genomic Analyses in R. *Molecular Biology
1048 and Evolution*, 31, 1929–1936. <https://doi.org/10.1093/molbev/msu136>

1049 Pinheiro, J., Bates, D., DebRoy, S., Sarkar, D., & R Core Team. (2021). *Nlme: Linear and
1050 Nonlinear Mixed Effects Models*. <https://CRAN.R-project.org/package=nlme>

1051 Pracana, R., Priyam, A., Levantis, I., Nichols, R. A., & Wurm, Y. (2017). The fire ant
1052 social chromosome supergene variant Sb shows low diversity but high divergence from SB.
1053 *Molecular Ecology*, 26(11), 2864–2879. <https://doi.org/10.1111/mec.14054>

1054 Price, A. L., Patterson, N. J., Plenge, R. M., Weinblatt, M. E., Shadick, N. A., & Reich, D.
1055 (2006). Principal components analysis corrects for stratification in genome-wide association
1056 studies. *Nature Genetics*, 38(8), 904–909. <https://doi.org/10.1038/ng1847>

1057 Purcell, S., Neale, B., Todd-Brown, K., Thomas, L., Ferreira, M. A. R., Bender, D., Maller,
1058 J., Sklar, P., Bakker, P. I. W. de, Daly, M. J., & Sham, P. C. (2007). PLINK: A Tool Set
1059 for Whole-Genome Association and Population-Based Linkage Analyses. *The American
1060 Journal of Human Genetics*, 81(3), 559–575. <https://doi.org/10.1086/519795>

1061 Ralph, P., Thornton, K., & Kelleher, J. (2020). Efficiently Summarizing Relationships in Large

1062 Samples: A General Duality Between Statistics of Genealogies and Genomes. *Genetics*,
1063 215(3), 779–797. <https://doi.org/10.1534/genetics.120.303253>

1064 Reich, D., Thangaraj, K., Patterson, N., Price, A. L., & Singh, L. (2009). Reconstructing Indian
1065 population history. *Nature*, 461(7263), 489–494. <https://doi.org/10.1038/nature08365>

1066 Renaut, S., Grassa, C. J., Yeaman, S., Moyers, B. T., Lai, Z., Kane, N. C., Bowers, J.
1067 E., Burke, J. M., & Rieseberg, L. H. (2013). Genomic islands of divergence are not
1068 affected by geography of speciation in sunflowers. *Nature Communications*, 4(1), 1827.
1069 <https://doi.org/10.1038/ncomms2833>

1070 Rhie, A., McCarthy, S. A., Fedrigo, O., Damas, J., Formenti, G., Koren, S., Uliano-Silva, M.,
1071 Chow, W., Fungtammasan, A., Kim, J., Lee, C., Ko, B. J., Chaisson, M., Gedman, G. L.,
1072 Cantin, L. J., Thibaud-Nissen, F., Haggerty, L., Bista, I., Smith, M., et al. (2021). Towards
1073 complete and error-free genome assemblies of all vertebrate species. *Nature*, 592(7856),
1074 737–746. <https://doi.org/10.1038/s41586-021-03451-0>

1075 Rubin, C.-J., Enbody, E. D., Dobreva, M. P., Abzhanov, A., Davis, B. W., Lamichhaney, S.,
1076 Pettersson, M., Sendell-Price, A. T., Sprehn, C. G., Valle, C. A., Vasco, K., Wallerman,
1077 O., Grant, B. R., Grant, P. R., & Andersson, L. (2022). Rapid adaptive radiation of
1078 Darwin's finches depends on ancestral genetic modules. *Science Advances*, 8(27), eabm5982.
1079 <https://doi.org/10.1126/sciadv.abm5982>

1080 Ruiz-Arenas, C., Cáceres, A., López-Sánchez, M., Tolosana, I., Pérez-Jurado, L., & González, J.
1081 R. (2019). scoreInvHap: Inversion genotyping for genome-wide association studies. *PLOS
1082 Genetics*, 15(7), e1008203. <https://doi.org/10.1371/journal.pgen.1008203>

1083 Sabeti, P. C., Reich, D. E., Higgins, J. M., Levine, H. Z. P., Richter, D. J., Schaffner, S.
1084 F., Gabriel, S. B., Platko, J. V., Patterson, N. J., McDonald, G. J., Ackerman, H. C.,
1085 Campbell, S. J., Altshuler, D., Cooper, R., Kwiatkowski, D., Ward, R., & Lander, E. S.
1086 (2002). Detecting recent positive selection in the human genome from haplotype structure.
1087 *Nature*, 419(6909), 832–837. <https://doi.org/10.1038/nature01140>

1088 Sabeti, P. C., Varilly, P., Fry, B., Lohmueller, J., Hostetter, E., Cotsapas, C., Xie, X., Byrne,
1089 E. H., McCarroll, S. A., Gaudet, R., Schaffner, S. F., Lander, E. S., Frazer, K. A., Ballinger,
1090 D. G., Cox, D. R., Hinds, D. A., Stuve, L. L., Gibbs, R. A., Belmont, J. W., et al. (2007).
1091 Genome-wide detection and characterization of positive selection in human populations.
1092 *Nature*, 449(7164), 913–918. <https://doi.org/10.1038/nature06250>

1093 Setter, D., Mousset, S., Cheng, X., Nielsen, R., DeGiorgio, M., & Hermisson, J. (2020).
1094 VolcanoFinder: Genomic scans for adaptive introgression. *PLOS Genetics*, 16(6), e1008867.
1095 <https://doi.org/10.1371/journal.pgen.1008867>

1096 Shao, C., Sun, S., Liu, K., Wang, J., Li, S., Liu, Q., Deagle, B. E., Seim, I., Biscontin, A.,
1097 Wang, Q., Liu, X., Kawaguchi, S., Liu, Y., Jarman, S., Wang, Y., Wang, H.-Y., Huang,
1098 G., Hu, J., Feng, B., et al. (2023). The enormous repetitive Antarctic krill genome
1099 reveals environmental adaptations and population insights. *Cell*, 186(6), 1279–1294.e19.
1100 <https://doi.org/10.1016/j.cell.2023.02.005>

1101 Shipilina, D., Pal, A., Stankowski, S., Chan, Y. F., & Barton, N. H. (2023). On the origin and
1102 structure of haplotype blocks. *Molecular Ecology*, 32(6), 1441–1457. <https://doi.org/10.1111/mec.16793>

1104 Singhal, S., Leffler, E. M., Sannareddy, K., Turner, I., Venn, O., Hooper, D. M., Strand,
1105 A. I., Li, Q., Raney, B., Balakrishnan, C. N., Griffith, S. C., McVean, G., & Przeworski,
1106 M. (2015). Stable recombination hotspots in birds. *Science*, 350(6263), 928–932. <https://doi.org/10.1126/science.aad0843>

1108 Smeds, L., Qvarnström, A., & Ellegren, H. (2016). Direct estimate of the rate of germline
1109 mutation in a bird. *Genome Research*, 26(9), 1211–1218. <https://doi.org/10.1101/gr.204669.116>

1111 Smukowski Heil, C. S., Ellison, C., Dubin, M., & Noor, M. A. (2015). Recombining without
1112 Hotspots: A Comprehensive Evolutionary Portrait of Recombination in Two Closely
1113 Related Species of *Drosophila*. *Genome Biology and Evolution*, 7(10), 2829–2842. <https://doi.org/10.1093/gbe/evv182>

1115 Speidel, L., Forest, M., Shi, S., & Myers, S. R. (2019). A method for genome-wide genealogy
1116 estimation for thousands of samples. *Nature Genetics*, 51(9), 1321–1329. <https://doi.org/10.1038/s41588-019-0484-x>

1118 Spence, J. P., & Song, Y. S. (2019). Inference and analysis of population-specific fine-
1119 scale recombination maps across 26 diverse human populations. *Science Advances*, 5(10),
1120 eaaw9206. <https://doi.org/10.1126/sciadv.aaw9206>

1121 Stern, A. J., Wilton, P. R., & Nielsen, R. (2019). An approximate full-likelihood method
1122 for inferring selection and allele frequency trajectories from DNA sequence data. *PLoS
1123 Genetics*, 15(9), 1–32. <https://doi.org/10.1371/journal.pgen.1008384>

1124 Steviston, L. S., Hoehn, K. B., & Noor, M. A. F. (2011). Effects of Inversions on Within-
1125 and Between-Species Recombination and Divergence. *Genome Biology and Evolution*, 3,
1126 830–841. <https://doi.org/10.1093/gbe/evr081>

1127 Steviston, L. S., Woerner, A. E., Kidd, J. M., Kelley, J. L., Veeramah, K. R., McManus, K.
1128 F., Great Ape Genome Project, Bustamante, C. D., Hammer, M. F., & Wall, J. D. (2016).
1129 The Time Scale of Recombination Rate Evolution in Great Apes. *Molecular Biology and
1130 Evolution*, 33(4), 928–945. <https://doi.org/10.1093/molbev/msv331>

1131 Tajima, F. (1989). Statistical method for testing the neutral mutation hypothesis by DNA
1132 polymorphism. *Genetics*, 123(3), 585–595. <https://doi.org/PMC1203831>

1133 Taylor, J. E. (2013). The effect of fluctuating selection on the genealogy at a linked site.
1134 *Theoretical Population Biology*, 87, 34–50. <https://doi.org/10.1016/j.tpb.2013.03.004>

1135 Todesco, M., Owens, G. L., Bercovich, N., Légaré, J.-S., Soudi, S., Burge, D. O., Huang, K.,
1136 Ostevik, K. L., Drummond, E. B. M., Imerovski, I., Lande, K., Pascual-Robles, M. A.,
1137 Nanavati, M., Jahani, M., Cheung, W., Staton, S. E., Muños, S., Nielsen, R., Donovan, L.
1138 A., et al. (2020). Massive haplotypes underlie ecotypic differentiation in sunflowers. *Nature*,
1139 584(7822), 602–607. <https://doi.org/10.1038/s41586-020-2467-6>

1140 Voight, B. F., Kudaravalli, S., Wen, X., & Pritchard, J. K. (2006). A Map of Recent Positive
1141 Selection in the Human Genome. *PLOS Biology*, 4(3), e72. <https://doi.org/10.1371/journal.pbio.0040072>

1143 Wakeley, J. (2008). *Coalescent Theory: An Introduction* (1st ed.). W. H. Freeman.

1144 Wakeley, J. (2020). Developments in coalescent theory from single loci to chromosomes.
1145 *Theoretical Population Biology*, 133, 56–64. <https://doi.org/10.1016/j.tpb.2020.02.002>

1146 Wellenreuther, M., & Bernatchez, L. (2018). Eco-Evolutionary Genomics of Chromosomal
1147 Inversions. *Trends in Ecology & Evolution*, 33(6), 427–440. <https://doi.org/10.1016/j.tree.2018.04.002>

1149 Wiuf, C., & Hein, J. (1999). Recombination as a Point Process along Sequences. *Theoretical
1150 Population Biology*, 55(3), 248–259. <https://doi.org/10.1006/tpbi.1998.1403>

1151 Wolf, J. B. W., & Ellegren, H. (2017). Making sense of genomic islands of differentiation in
1152 light of speciation. *Nature Reviews Genetics*, 18(2), 87–100. <https://doi.org/10.1038/nrg.2016.133>

1154 Yi, X., Liang, Y., Huerta-Sanchez, E., Jin, X., Cuo, Z. X. P., Pool, J. E., Xu, X., Jiang, H.,
1155 Vinckenbosch, N., Korneliussen, T. S., Zheng, H., Liu, T., He, W., Li, K., Luo, R., Nie,
1156 X., Wu, H., Zhao, M., Cao, H., et al. (2010). Sequencing of 50 Human Exomes Reveals
1157 Adaptation to High Altitude. *Science*, 329(5987), 75–78. <https://doi.org/10.1126/science.1190371>